Integrated Master on Chemical Engineering

# *Numerical Studies of Dispersion in Packed Beds of Spherical Particles*

## Master Thesis

of

**Paulo Miguel Oliveira Cardoso do Carmo**

**Developed for the course of Dissertação**

in

IFP Énergies Nouvelles


Supervisor at FEUP: **Prof. Madalena Maria Gomes de Queiroz Dias**

Supervisor at IFPen: **Cláudio António Pereira da Fonte PhD**

**Aude Royon-Lebeaud PhD**


**Department of Chemical Engineering**

**June of 2016**

# Acknowledgements

Before anything else, I would like to thank everyone that has helped me during this thesis and whose name I did not write here.

First of all, I would like to thank M. Dominique Humeau, director of the Process Experimentation division, and M. Herve Cauffriez, department head of the Experiment Intensification department, for making my internship and thesis possible.

To my supervisor from FEUP, Prof. Madalena Dias I am forever grateful for all her experience, work and patience. This project would not have been possible without her help.

To my supervisors in IFPEN, Cláudio António Pereira da Fonte PhD and Aude Royon-Lebeaud PhD, I would like to thank for all their help, availability, kindness and motivation. And for always correcting my many mistakes.

I would like to thank my fellow trainees in IFPEN, for all the support and comradery that you showed me. Thank you for all the pleasant memories.

To my colleagues Gonçalo Santos and David de Oliveira, I'm grateful that we were on this together and that thank you for sharing your adventure in Lyon with me.

To my closest friends and family, thank you for the love, support and worries and for letting me take this great opportunity.

---

Prof. Madalena Dias, supervisor of this work, is a member of the Associate Laboratory LSRE-LCM, funded by Project POCI-01-0145-FEDER-006984, *Fundo Europeu de Desenvolvimento Regional* (FEDER) through COMPETE2020 - Programa Operacional Competitividade e Internacionalização (POCI), and by national funds through FCT - Fundação para a Ciência e a Tecnologia.

# Resumo

Neste trabalho são criadas simulações CFD de uma coluna de enchimento com partículas esféricas com o objetivo de determinar os coeficientes de dispersão para o Xileno a uma temperatura de 170 °C com $Sc = 29$.

Um empacotamento de esferas é obtido recorrendo ao método de elementos discretos e utilizado para representar um meio poroso tridimensional. Simulações numéricas diretas tridimensionais são utilizadas para recrear experiências de determinação de $Pe_L$ e $Pe_T$ a diferentes $Pe_m$ e os resultados comparados com correlações existentes. Os domínios 3D mostraram-se adequados para simular o escoamento no leito fixo, mas não possuíam o tamanho ideal para a determinação de $Pe_T$.

Foram ainda utilizadas técnicas de processamento de imagem para estudar e extrair o perfil de porosidade radial a partir de tomografias axiais computorizadas de uma coluna de leito fixo real. Este perfil de porosidade é então utilizado numa simulação 2D axissimétrica equivalente e comparado a um segundo perfil encontrado na literatura em termos de número de reatores agitados desenvolvidos pelo leito fixo equivalente.

A influência dos valores dos números de Péclet transverso e axial no número de reatores perfeitamente agitados ao longo de um leito fixo equivalente é também estudado: comparação entre Gunn (1969) e Guedes de Carvalho e Delgado (2005), estimativa de $Pe_m$ a partir de uma velocidade intersticial média e local.

Os resultados principais são:

- Os resultados válidos para $Pe_T$ estão de concordo com a correlação de Gunn (1969);
- Os resultados obtidos para $Pe_L$ não respeitam as imposições do método usado inicialmente. Um método alternativo foi usado e o $Pe_L$ obtido mostra uma boa concordância com a correlação de Gunn (1969);
- Observa-se uma forte influência do perfil de porosidade (número mais elevado de reatores perfeitamente agitados com o perfil de porosidade obtido por tomografia axial computorizada;
- Influência de segunda ordem de Péclet no alcance proposto por Gunn (1969) e Guedes de Carvalho and Delgado (2005). Os maiores valores de $Pe_T$, menos difusivos, induzem para um menor número de reatores perfeitamente agitados
- Influência de terceira ordem da velocidade na estimação de $Pe_T$ devido à baixa variação de $Pe_T$ com $Pe_m$.

**Keywords:** CFD; Packed Bed; Dispersion Coefficient
3D DNS; 2D axisymmetric

# Abstract

In this study, CFD simulations of a packed column with spherical particles are created to determine the dispersion coefficients for Xylene at a temperature of 170 ºC with a $Sc = 29$.

A packing of spheres is obtained using a Discrete Element Method and used to represent a 3D porous media. 3D Direct Numerical Simulations are used to recreate experiences for the determination of $Pe_L$ and $Pe_T$ at different $Pe_m$ and the results are compared with existing correlations. The 3D domains proved adequate to simulate the flow of the packed bed, but didn't have the ideal size for the determination of the $\mathrm{Pe_T}$.

Additionally, image processing techniques are used to study and extract the radial porosity profile from CAT scans of a real packed column. This porosity profile is then used in an equivalent 2D axisymmetric simulation and compared with another porosity profile found in literature in terms of number of CSTR developed by the equivalent packed bed.

The influence of values of transverse and axial Péclet on the number of CSTR along an equivalent packed bed is also studied : Gunn (1969) versus Guedes de Carvalho and Delgado (2005), estimation of the $Pe_m$ with a mean instertitial velocity or a local value of the interstitial velocity.

The main results are:

- The validated results for $Pe_T$ showed a good agreement with the correlation of Gunn (1969);
- The obtained results for $Pe_L$ did not comply with the initial used method requirements. An alternative method was used and the resulting $Pe_L$ show a good agreement with the correlation of Gunn (1969);
- Strong influence of the porosity profile (higher number of CSTR with the porosity profile from CAT);
- Influence of the second order of the Péclet in the range proposed by the correlation of Gunn (1969) and Guedes de Carvalho and Delgado (2005). The higher values of $Pe_T$, less diffusive, induce to a lower number of CSTR;
- Influence of the third order of the velocity retained in the estimation of the $Pe_T$ because of the small range of variation of the $Pe_T$ with the molecular Péclet.

# Declaration

I hereby certify and declare on my honor that the present work is my own and everything coming from external sources has been properly referenced.

4th of July of 2016

# Indices

# Notation e Glossary

| | | |
|---|---|---|
| $Sc$ | Schmidt Number | |
| $D_m$ | Molecular Diffusivity | $m^2/s$ |
| $D_L$ | Longitudinal Dispersion Coefficient | $m^2/s$ |
| $D_T$ | Transverse Dispersion Coefficient | $m^2/s$ |
| $Pe_m$ | Molecular Péclet Number | |
| $Pe_L$ | Longitudinal Péclet Number | |
| $Pe_T$ | Transverse Péclet Number | |
| $P_{ef}$ | Fluid Mechanical Péclet Number | |
| $Pe_{eq}$ | Equivalent Péclet Number | |
| $u$ | Interstitial velocity | $m/s$ |
| $U$ | Superficial velocity | $m/s$ |
| $d_p$ | Mean Particle Diameter | $m$ |
| $C$ | Species Concentration | |
| $z$ | Longitudinal Direction | $m$ |
| $x$ | Transverse Direction | $m$ |
| $Z$ | Normalized Longitudinal Direction by the mean particle diameter | |
| $X$ | Normalized Transverse Direction by the mean particle diameter | |
| $L$ | Length of the column | $m$ |
| $\Delta P$ | Pressure Drop | $Pa$ |
| $Re$ | Reynolds Number | |
| $\alpha_1$ | First Root of the Zero-Order Bessel Function | |
| $J$ | Equivalent Number of CSTR | |

*Greek letters*

| | |
|---|---|
| $\epsilon$ | Void fraction of the packed bed |
| $\sigma$ | Standard deviation |
| $\tau$ | Tortuosity factor |
| $\mu$ | Viscosity |
| $\rho$ | Mass Density |

***Acronyms List***

| | |
|---|---|
| CFD | Computational Fluid Dynamics |
| DNS | Direct Numerical Simulation |
| CAT | Computational Axial Tomography |
| CSTR | Continuously Stirred Tank Reactor |

# 1 Introduction

## 1.1 Project Presentation

Over the past seven decades, packed beds have been used in several applications of petroleum and chemical industries, involving reaction and separation. Packed beds have been the subject of continuous research towards increased efficiency of existing equipment or the development of new ones. They can be generalized as a solid vessel filled with a packing material that can range from a solid catalyst to be used in a heterogeneous reaction, an inert filling to promote mixing, and an adsorbent for separation of multi-component liquid or gaseous effluents.

One of the fundamental interests in this area is the characterization of the hydrodynamics of porous media flow and the estimation of dispersion coefficients involved in the transport of chemical species along the packed bed, in a way that enables an accurate prediction of the output of this equipment. Different procedures can be used to obtain these dispersion parameters. When available in the literature, previously developed correlations can be used to estimate these values. Alternatively, experimental testing can be performed if there is a lack of information regarding the system or if there is a need to re-evaluate certain correlations due to the development of new devices, or from conflicting experimental results. However, not all experimental conditions can be easily reproduced. Extreme temperatures and pressures and dangerous reagents can limit the number of tests and quality of the possible experimental data. With recent advances of computation technology, Computational Fluid Dynamics (CFD) simulations can be used to predict these parameters with increasing precision. As mentioned in Augier et al (2010) “The use of numerical simulation can provide an important gain of time and should limit the number of experiments. Another reason to use CFD is to access information at the local scale, which is generally not (or hardly) measurable with experimental methods”.

## 1.2 Company Presentation

IFP Energies nouvelles (IFPEN) is a major research and training player in the fields of energy, transport and the environment. From research to industry, technological innovation is central to all its activities.

As part of the public-interest mission with which it has been tasked by the public authorities, IFPEN focuses on:

- providing solutions to take up the challenges facing society in terms of energy and the climate, promoting the transition towards sustainable mobility and the emergence of a more diversified energy mix;
- creating wealth and jobs by supporting French and European economic activity, and the competitiveness of related industrial sectors.

Its programs are structured around 3 strategic priorities:

- **Sustainable mobility**: developing effective, environmentally-friendly solutions for the transport sector;
- **New energies**: producing fuels, chemical intermediates and energy from renewable sources;
- **Responsible oil and gas**: proposing technologies that meet the demand for energy and chemical products while improving energy efficiency and reducing the environmental impact.

An integral part of IFPEN, its graduate engineering school – IFP School – prepares future generations to take up these challenges.

## 1.3 Contributions to the Art

In this work, dispersion data was obtained for a Schmidt number ($Sc = 29$) not yet studied in previous literature. 3D direct numerical simulations (DNS) were done to recreate Han's (1985) experiments for the determination of the transversal and longitudinal dispersion coefficients. With an image processing software, a radial porosity profile was obtained from CAT scans of a real porous bed and the resulting profile was fitted to Giese's mathematical correlation. An equivalent 2D porous media was created, the influence of the local velocity was studied in the value of $Pe_m$.

## 1.4 Thesis Organization

1) Develop a 3D model of a representative section of a packed bed to obtain through direct numeric simulation (DNS) the dispersion coefficients for the flow of a specific fluid with a known Schmidt number $(Sc \sim 29)$, which is outside the range of the normal experimental points in previous works.
2) Obtain the radial distribution of porosity from CAT images, through imaging processing, using Matlab. Develop a 2D axisymmetric model of the flow to study near-wall channeling effects

# 2 State of The Art on Modeling of Confined Packed Bed as an Equivalent Porous Media

## 2.1 Mass Dispersion in Packed beds

### 2.1.1 Theory

Molecular diffusivity, $D_m$, is a property of the fluid that appears commonly associated with the use of transport equations based on Fick's law and can be described as the constant ratio between the molar flux through the fluid and the concentration gradient of a specie.

In this work, adequate dispersion coefficients take the place of the previous molecular diffusion: the longitudinal dispersion coefficient $D_L$ that accounts for the diffusion and the advective mixing effects in the direction of the flow; and transverse dispersion coefficient $D_T$ that accounts for the cross-stream dispersion. In each case, both coefficients are used in the modeling of an equivalent porous medium.

At low fluid velocities, dispersion is ruled solely by molecular diffusion with $D_L = D_T = D_m/\tau$, with $\tau$ being the porous medium tortuosity. At high fluid velocity, a state described by Coelho and Guedes de Carvalho (1988) as "fluid mechanical" is observed in which, the values of longitudinal Péclet number $\left(Pe_L = ud_p/D_L\right)$ and transverse Péclet number $\left(Pe_L = ud_p/D_L\right)$ tend to constant values ( $Pe_L(\infty) = 2$ ; $Pe_T(\infty) = 12$).

For intermediate fluid velocities, $Pe_T$ and $Pe_L$ can be estimated by the sum of the contributions of the molecular diffusion and the advective mixing effects. This is given by Equations (1) and (2), which give $Pe_T$ and $Pe_L$ as a function of the molecular Péclet number $\left(Pe_m = ud_p/D_m\right)$, and usually used to estimate dispersion coefficients in flows of gases in porous media ($Pe_m \sim O(1)$) or liquids with a high value of $Pe_m$ ($\sim O(10^4)$)

$$\frac{1}{Pe_T} = \frac{1}{\tau}\frac{1}{Pe_m} + \frac{1}{12} \tag{1}$$

$$\frac{1}{Pe_L} = \frac{1}{\tau}\frac{1}{Pe_m} + \frac{1}{2} \tag{2}$$

Equations (1) and (2) fail, however, to properly describe flows with intermediate $Pe_m$ (Guedes de Carvalho, J.R.F. and Delgado, 2005)

Beyond Equations (1) and (2), dispersion coefficients can also be estimated by fitting experimental data to the following mass balance, and in this work through the method of Han (1985)

$$\frac{\partial C}{\partial t} = -u\frac{\partial C}{\partial z} + D_L\frac{\partial^2 C}{\partial z^2} + D_T\frac{\partial^2 C}{\partial x^2} \tag{3}$$

where $u$ is the interstitial velocity, $C$ is the concentration of a species, $z$ is the distance in the axial direction, $x$ is the distance in the transverse direction and $t$ is the time. Rewriting Equation (1) and introducing the Péclet number:

$$\tau_p\frac{\partial C}{\partial t} = -\frac{\partial C}{\partial Z} + \frac{1}{Pe_L}\frac{\partial^2 C}{\partial Z^2} + \frac{1}{Pe_T}\frac{\partial^2 C}{\partial X^2} \tag{4}$$

where $\tau_p = d_p/u$ is the mean particle time, the time it takes for the fluid to cross a distance equal to the mean particle diameter and $Z$ and $X$ are the distance in the longitudinal and transverse direction normalized by the mean particle diameter $\left(Z = z/d_p\ ; X = x/d_p\right)$.

In this work, CFD will be used to calculate the dispersion coefficients in a randomly and isotropic packed bed for a specific fluid with given Schmidt number

$$Sc = \frac{\mu}{\rho D_m} \tag{5}$$

where $\mu$ is the viscosity and $\rho$ is the density. The Schmidt number is a dimensionless coefficient that relates the viscous diffusion rate to the molecular diffusion rate. Typical values include $Sc = O(1)$ for gases and $Sc{\sim}O(10^3)$ for liquids. Systems with $Sc$ number within this range often share physical properties of the two states and can be especially difficult to characterize.

In this work, particular attention will be given to systems with $Sc = 29$, the recorded value for a stream of xylene at a temperature of 170ºC. Upon gathering correlations from the literature, discrepancies between different authors, specially *Guedes de Carvalho and Delgado (2005)* and *Gunn (1969)* were noticed for the $Sc$ number range of interest, especially for the estimation of the $Pe_T$, which could differ by $\sim 20$.

### 2.1.1 Transverse Dispersion

#### 2.1.1.1 Description of Han's experiment

Experimental conditions can be adapted for the determination of the transverse dispersion coefficient. Using the conditions of Han's (1985) lateral dispersion experiment (Figure 1), in which the gradients of concentration on the axial direction are negligible $D_L\frac{\partial C}{\partial x} \approx 0$, since the layer for mass transfer in the axial direction is much smaller than the axial distance ($L$). In steady-state $\left(\frac{\partial C}{\partial t} = 0\right)$ and with a symmetry boundary condition to remove the no-slip

condition at the limits of the domain, a tracer inlet with a step profile in concentration will result in the smoothening of the concentration gradient along the transversal direction and Equation (4) can be solved to give the radial profile of the concentration:

$$\frac{C}{C_0} = \frac{1}{2}\,\mathrm{erfc}\left(\frac{x}{2\sqrt{zD_T/u}}\right) \tag{6}$$

which in turn can be rearranged as a function of the normalized distances by the mean particle diameter and the Péclet number, as follows

$$\frac{C}{C_0} = \frac{1}{2}\,\mathrm{erfc}\left(\frac{x/d_p}{2\sqrt{\frac{z}{d_p Pe_T}}}\right) \tag{7}$$

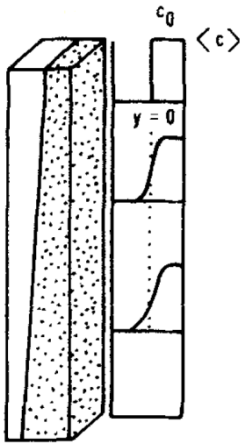


*Figure 1: Han's Lateral Dispersion experiments to calculate* $\boldsymbol{D_T}$*. (Han et al., 1985)*

#### 2.1.1.2 Validity condition for Han's experiments

Equation (7) can only be applied with confidence if the collected data is taken from a section in which the flow is properly developed. (Augier et al., 2010) For that purpose, Equation (8) states that the normalized distance in z direction by the mean particle diameter for which the flow is properly developed is a function of the transversal Péclet number and the porosity:

$$Z \gg Pe_T \frac{\varepsilon}{1-\varepsilon} \tag{8}$$

#### 2.1.1.3 Comparison of available data in the literature

A vast number of authors have contributed with experimental data for the determination of dispersion coefficients in granular packed beds, some with a contribution of data and comparison existing correlations and others with their own proposed correlations. For the sake of convenience, all experimental data comparisons will be referred to Guedes de

Carvalho and Delgado (2005), in which a significant number of data from other sources has been compiled and analyzed.

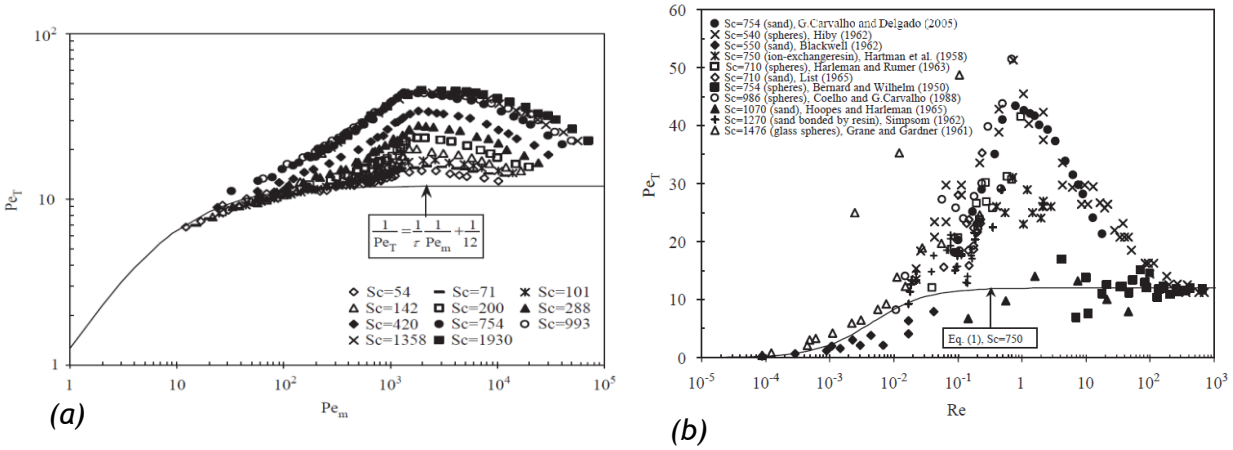


Figure 2: *Data collected by Guedes de Carvalho and Delgado (2005) (a) and a comparison to the data obtained by other authors (b) with* $Pe_T$ *plotted as a function of* $Re\ (= Pe_m \varepsilon / Sc)$

Figures 2(a) and 2(b) show examples of various sets of data for the transverse dispersion from different authors and for different $Sc$, taking into special attention the values relating to the $Sc$ of 54, the closest value of available to the value studied in this work.

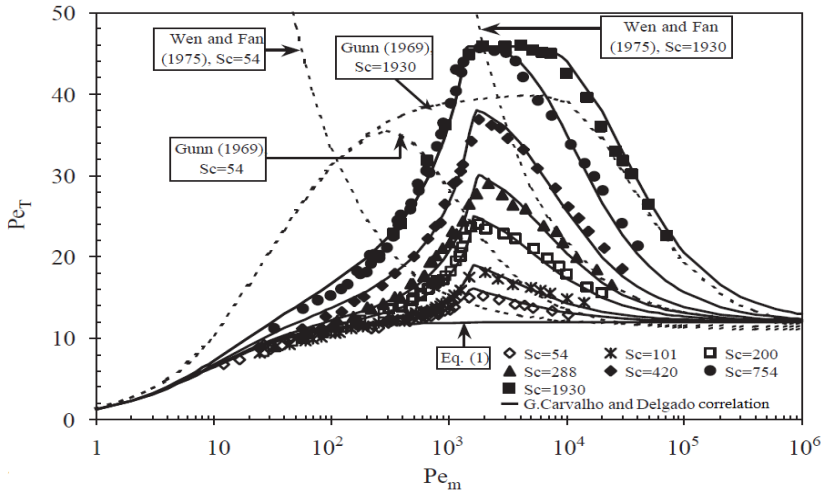


*Figure 3: Comparison of the data obtained in Guedes de Carvalho and Delgado (2005) with other existing correlations*

Figure 3 shows a comparison of the experimental data obtained by Guedes de Carvalho and Delgado (2005) and three different correlations, one proposed by the same authors as a result of this experiments, another from Gunn (1969) and a third from Wen and Fan (1975) for extreme $Sc$ values. From Figures 3(a) and 3(b), in order to have a second reference to use as a guide line for this case, the correlations of Guedes de Carvalho and Delgado (2005) and Gunn (1969) are chosen to as references for the CFD experiments.

Extrapolations for each correlation for $Sc = 29$ are represented in Figure 4.

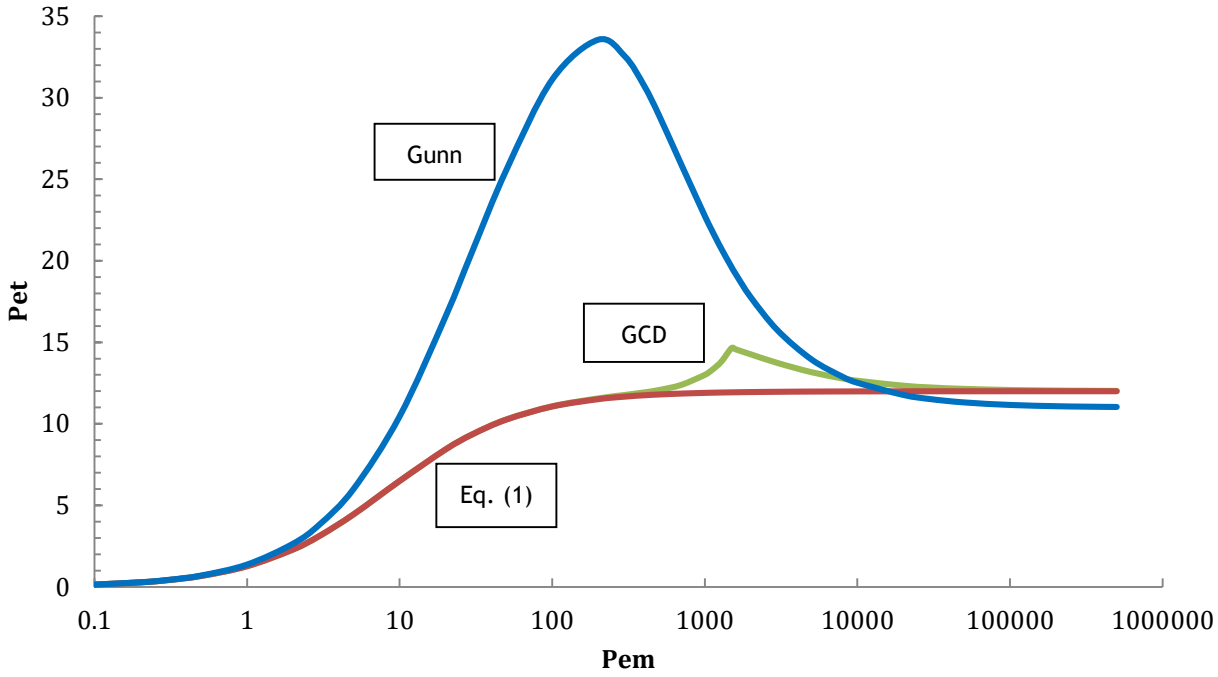


*Figure 4: Comparison of the correlations of Guedes de Carvalho and Delgado (2005) (GCD), Gunn (1969) (Gunn) and Equation (1), for a $Sc$ of 29 for the transversal Péclet*

Gunn (1986) suggests the following correlation for the estimation of transverse dispersion coefficients

$$\frac{1}{Pe_T} = \frac{1}{Pe_f} + \frac{1}{\tau}\frac{1}{Pe_m} \tag{9}$$

where the fluid-mechanical Péclet is given by $P_{ef} = 40 - 29e^{-7/Re}$ with the Reynolds number given by $Re = \frac{P_{em}\varepsilon}{Sc}$.

For Schmidt numbers smaller than 550, Guedes de Carvalho and Delgado (2005) suggest the following correlations

$$\frac{1}{Pe_T} = \frac{1}{\tau}\frac{1}{Pe_m} + \frac{1}{12} - \left(\frac{Sc}{1500}\right)^{4.8}(\tau Pe_m)^{3.83-1.3\log_{10}(Sc)} \qquad Pe_m < 1600 \tag{10}$$

$$Pe_T = (0.058\,Sc + 14) - (0.058\,Sc + 2)e^{-\frac{352\,Sc^{0.5}}{Pe_m}} \qquad Pe_m > 1600 \tag{11}$$

### 2.1.2 Axial Dispersion

#### 2.1.2.1 Description of Han's experiment

The longitudinal dispersion coefficient can be calculated by returning to the initial mass conservation equation, Equation (4), and by following the conditions of Han's (1985) longitudinal dispersion experiment (Figure 7), the transversal dispersion will be negligible $D_T \frac{\partial C}{\partial x} \approx 0$ since there is no concentration gradient in the transversal direction. In transient state and with symmetry boundary conditions, a response to a pulse input in concentration will result in the smoothening of the inlet concentration gradient along the longitudinal direction and the following analytical solution

$$\frac{C}{C_0} = \frac{1}{2}\,\mathrm{erfc}\left(\frac{z-ut}{2\sqrt{D_L t}}\right) + \frac{1}{2}\,e^{\frac{uz}{D_L}}\mathrm{erfc}\left(\frac{z+ut}{2\sqrt{D_L t}}\right) \tag{12}$$

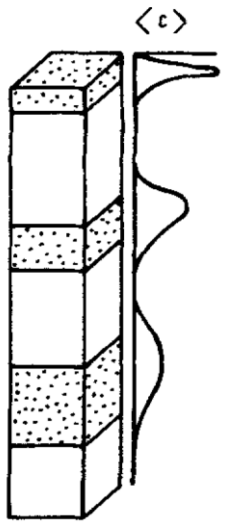


*Figure 5: Han's Step experiment to calculate $\boldsymbol{D_L}$. (Han et al., 1985)*

#### 2.1.2.2 Validity condition for Han's experiments

Equation (12) is only valid if the following criterion is verified (Augier et al., 2010)

$$Z \gg Pe_L \frac{\varepsilon}{1-\varepsilon} \tag{13}$$

Equation (12) states that the normalized distance by the mean particle diameter in the z axis or the depth of the column ($Z$) for which the flow is fully developed and therefore capable to obtain a proper tracer response curve from, is a function of the porosity and the longitudinal Péclet number.

### 2.1.2.3 Comparison of available data in the literature

In Figures 6(a) and 6(b) various sets of data for different authors and different $Sc$ are compared this time to determine the longitudinal dispersion, special attention is drawn to the values of $Sc$ of 54 from Guedes de Carvalho and Delgado (2005) and $Sc$ of 9.1 the two values closest to the pretended case.

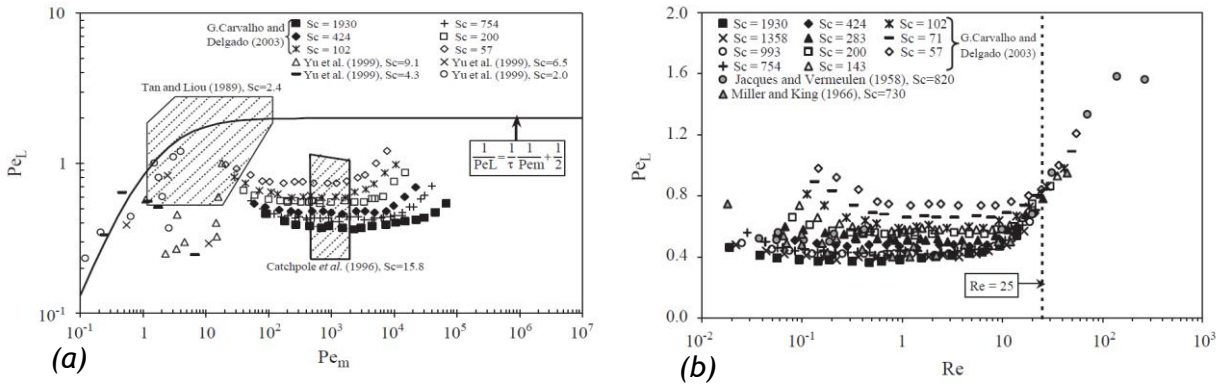


*Figure 6: Experimental data for the longitudinal dispersion from different authors with $Pe_L$ plotted as a function of $Pe_m$* (a) *and $Re$* (b)

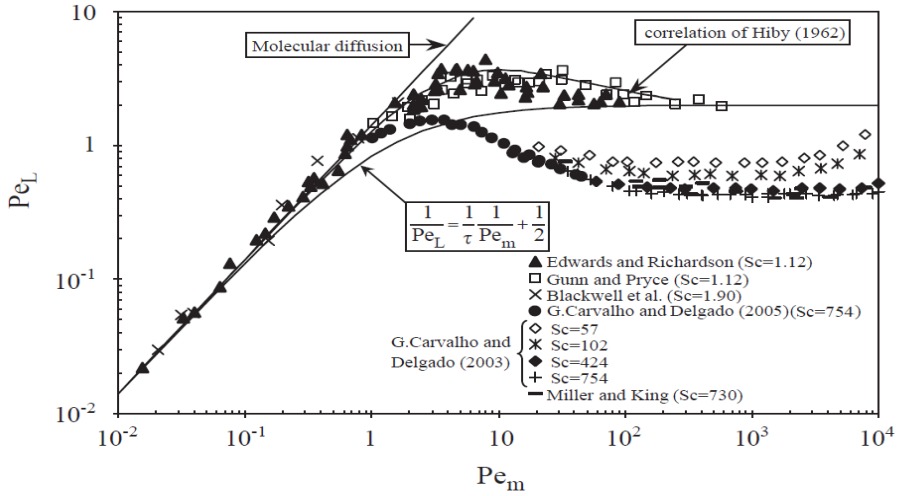


*Figure 7: Comparison of the data collected of $Pe_L$ from Guedes de Carvalho and Delgado (2005) and other authors*

From the four correlations available: Guedes de Carvalho and Delgado (2005), Edward and Richardson (2005), Gunn and Pryce and Blackwell et al. (2005), the correlations of Guedes de Carvalho and Delgado (2005) and Gunn and Pryce are being used to establish a reference for the CFD experiments. The extrapolation of the proposed correlations for $Sc = 29$ are displayed in Figure 8.

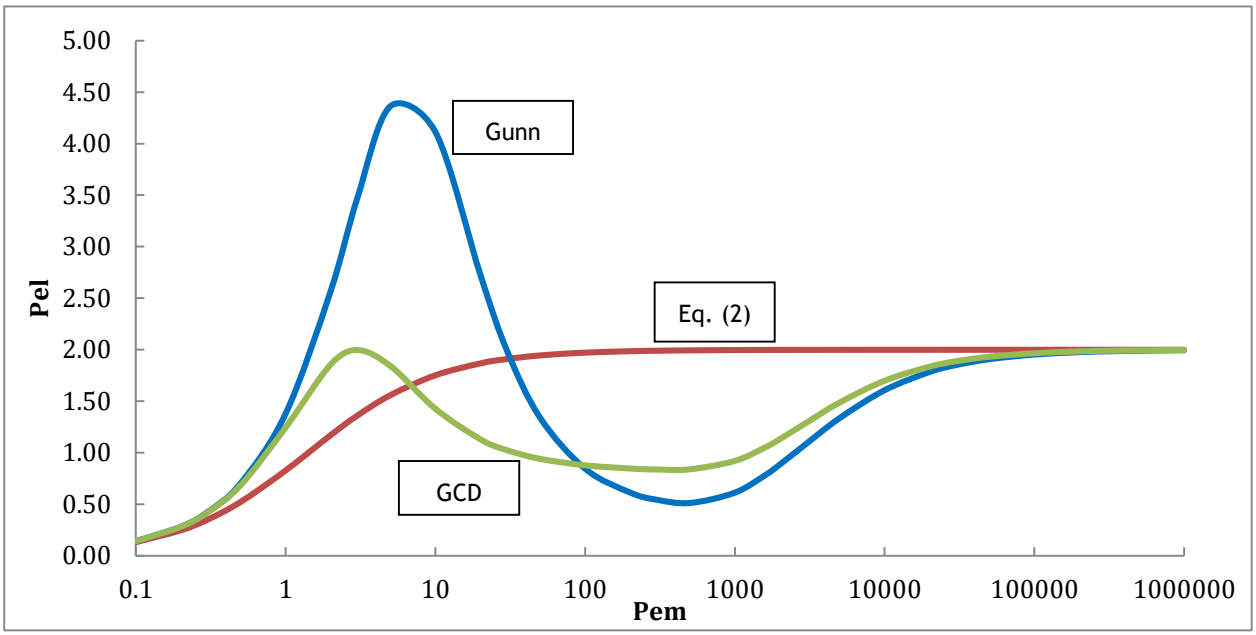


*Figure 8: Comparison of the correlations of Guedes de Carvalho and Delgado (2005) (GCD), Gunn (1969) (Gunn) and Equation (2), for a $Sc$ of 29 for the longitudinal Péclet*

For axial dispersion, Gunn (1986) suggested the following correlation, based on the probability $p$ of a tracer particle either remaining at rest, or travelling a distance downstream in the space of the characteristic time interval. (Gunn, 1986)

$$\frac{1}{Pe_L} = \frac{Re\,Sc}{4\alpha_1^2(1-\varepsilon)}(1-p)^2 + \frac{Re^2\,Sc^2}{16\alpha_1^4(1-\varepsilon)^2}p(1-p)^3\left(e^{\frac{-4(1-\varepsilon)\alpha_1^2}{p(1-p)ReSc}} - 1\right) + \frac{\varepsilon}{\tau ReSc} \qquad (14)$$

where $\alpha_1$ is the first root of the zero-order Bessel function, $\varepsilon$ is the void fraction of the packed bed and $p$ is dependent on the geometry of the particle, and for spherical particles is given by

$$p = 0.17 + 0.33e^{\frac{-24}{Re}}, \tau = 1.4 \qquad (15)$$

Guedes de Carvalho and Delgado (2005) proposes another equation with a different dependency of $p$ on $Sc$

$$\frac{1}{Pe_L} = \frac{Pe_m}{5}(1-p)^2 + \frac{Pe_m^2}{25}p(1-p)^3\left(e^{\frac{-5}{p(1-p)Pe_m}} - 1\right) + \frac{\varepsilon}{\tau Pe_m} \qquad (16)$$

$$p = \frac{0.48}{Sc^{0.15}} + \left(\frac{1}{2} - \frac{0.48}{Sc^{0.15}}\right)e^{-\frac{75Sc}{Pe_m}} \qquad (17)$$

However, from a review of previous works, there seems to be a lack of experimental data in the range of $Sc$ between the values of 2 and 550. Guedes de Carvalho and Delgado (2001)

reported additional data for dispersion coefficients in the range $50 < Sc < 550$. Nonetheless, that still leaves out the interval $2 < Sc < 50$ for which does not exist experimental values for comparison. Since the purpose of this work is to study the flow and dispersion of a liquid with $Sc = 29$, it will try to fill this void.

### 2.1.3 Direct Numerical Simulations (DNS)

A DNS approach requires the a complete numerical solution of the Navier-Stokes equations without additional models (Baker, 2011) and allows for a localized study of the dispersion phenomenon at particle scale. This approach is generally used when there is no other viable model to accurately represent the study case or when the objective of the simulation is to check the veracity of another model, without the need to physically perform an experiment. The only limit is the dependence on the quality and refinement of a numerical mesh. As a natural consequence of this need, a DNS has a much higher computational cost than a model based approach such as the Reynolds-averaged Navier-Stokes equations (RANS) or the Large Eddy Simulation (LES), a situational aggravated when dealing with packed beds, because it's necessary to solve all flow length scales, down to the scale of the pores of the packed bed.

A CFD DNS model of the flow in a porous medium was developed in this work to reproduce Han's experiments and attempt to obtain $D_T$ and $D_L$ data for a $Sc$ of 29.

## 2.2 Porosity Profiles in Confined Packed Beds

In the presence of walls, the stacked particles suffer a rearrangement in their packing, this phenomena, showed in Figure 10, the near-wall channeling effect, alters the porosity on a local scale and is dependent on the ratio of $D/d_p$.

For large values of $D/d_p$ (>20), the effect is only shown on a small length of the radial distance and can be neglected, since it will not have a significant impact on the columns hydrodynamics. For a small ratio of $D/d_p$ (<10), this effect cannot be ignored since it will impact the columns velocity profile, as showed in Figure 10. A precise characterization of the porosity profile is needed for modeling the flow in a highly-confined packed bed (typically $D/d_p$<10).

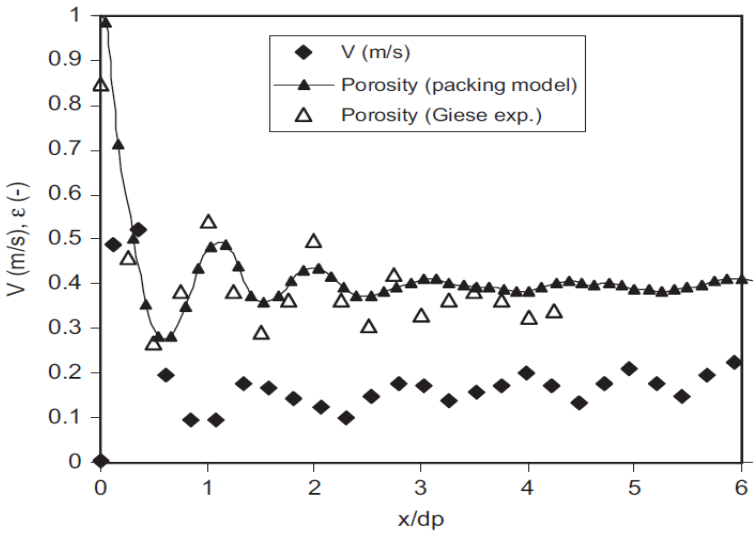


*Figure 9: Example of porosity and velocity profiles versus distance from the wall (Augier et al., 2010)*

In this pursuit, Computational Axial Tomography, CAT, scans were used to determine radial porosity profile in a column of diameter $D = 7\ mm$ filled with glass spheres with a diameter $d_p = 0.56\ mm$ The images obtained from a specialized CAT machine were converted into binary images, as a first treatment to separate the particles (value of 1) from the void (value of 0).

The images are analyzed with an image processing software to determine the sensibility and number requirements to obtain satisfactory values of porosity through this method and finally to obtain the requested plot of the porosity as a function of the distance from the wall.

# 3 3D Direct Numerical Simulations

## 3.1 Domain generation

### 3.1.1 Grains3D

In order to create a computational domain for DNS, a Discrete Elements Method (DEM) code, Grains3D, developed at IFPen and specially designed to simulate the packing of spheres was used. A simulation was made of the packing of glass spheres in a container with periodic boundary conditions, which guarantees the absence of the near-wall porosity effects. (Wachs et al., 2012)

### 3.1.2 Required Dimensions of the computational Domain

The first step consists in determining the necessary dimension of the computational domain and the position of the section from which the computational data will be gathered. to obtain this, different criterions will be used.

To observe a fully developed velocity profile, a minimum distance on the $z$ axis from the inlet must be respected. For this work this distance will be considered equal to three times the mean particle diameter, and, if needed, will be altered according to the results

$$Z_{min,1} = 3 \tag{18}$$

To select the ideal section of the mesh for each analysis of the transversal coefficient, it must be ensured that the transversal distance from the center of the domain to the symmetry boundary is enough so that the dispersive concentration front does not reach it. This condition must be ensured so that Equation (7) can be fitted to the breakthrough curves to determine $P_{eT}$. This distance depends on the chosen $P_{eT}$ and will change accordingly.

Equation (7) is resolved using the exterior symmetry boundary conditions, since the initial interface between the fluid and the tracer is situated in the middle of the x axis to guarantee a symmetry between the two diffusive fronts, the origin of the axis will be moved to that symmetry, resulting in the following conditions: $X = X_{max} = 10\,,\ C = 0$.

$$\operatorname{erfc}\left(\frac{X_{max}}{2\sqrt{\frac{Z}{Pe_T}}}\right) = 0 \tag{19}$$

Studying the complementary error function, it can be observed that for a range of x values equal or greater than 2, for which the tracer concentration is only 0.5% of the injecting concentration. Equation (19) is respected resulting in the following approximation

$$\frac{X_{max}}{2\sqrt{\frac{Z}{Pe_T}}} \geq 2 \tag{20}$$

$$Z_{max,1} \leq Pe_T \left(\frac{X_{max}}{4}\right)^2 \tag{21}$$

As previously referred, fitting data from Han's (1985) experiments to Equation (7) holds true if some constraints are respected. The first constraint can be established as follows:

$$Z_{min,2} = Pe_T \frac{\varepsilon}{1-\varepsilon} \tag{22}$$

According to Equation (8) the $Z$ distance for the data collection must be one order bigger than $Z_{min,2}$. A parameter $N$ will be defined to account for this, and its effect will be studied.

$$Z = N\, Z_{min,1} = NPe_T \frac{\varepsilon}{1-\varepsilon} \tag{23}$$

For this work the parameter $N$ was given a starting value $N = 9$, so it was high enough to satisfy Equation (8) while respecting Equation (21). The influence of $N$ will also be studied for the obtained result.

From the above stipulated constraints, Equations (18), (21), (22) and (23), the necessary mesh dimensions and the location of the ideal section of the mesh to analyze have been determined for a $N = 9$ and are listed in Table 1.

*Table 1: Ideal dimensions of the mesh by* $\boldsymbol{Pe_T}$

| $\boldsymbol{Pe_T}$ | $\boldsymbol{Z_{min,1}}$ | $\boldsymbol{Z_{min,2}}$ | $\boldsymbol{Z}$ | $\boldsymbol{Z_{max,1}}$ |
|---|---|---|---|---|
| **0,1** | 3 | 0,06 | 0,61 | 0,63 |
| **0,3** | 3 | 0,18 | 1,83 | 1,88 |
| **0,5** | 3 | 0,31 | 3,05 | 3,13 |
| **0,7** | 3 | 0,43 | 4,27 | 4,38 |
| **1** | 3 | 0,61 | 6,10 | 6,25 |
| **3** | 3 | 1,83 | 18,31 | 18,75 |
| **5** | 3 | 3,05 | 30,52 | 31,25 |
| **7** | 3 | 4,27 | 42,72 | 43,75 |
| **10** | 3 | 6,10 | 61,03 | 62,50 |
| **13** | 3 | 7,93 | 79,34 | 81,25 |
| **15** | 3 | 9,15 | 91,55 | 93,75 |
| **17** | 3 | 10,38 | 103,75 | 106,25 |
| **20** | 3 | 12,21 | 122,06 | 125,00 |
| **23** | 3 | 14,04 | 140,37 | 143,75 |
| **27** | 3 | 16,48 | 164,78 | 168,75 |
| **30** | 3 | 18,31 | 183,09 | 187,50 |
| **33,5** | 3 | 20,45 | 204,45 | 209,38 |

To be able to measure $Pe_T$ up to 33.5, a domain with the size 20×3×200 particles is required. However, due to computational limitations, the proposed domain is too big to be generated with the chosen DEM code. A domain with 20×3×100 particles was generated instead, allowing the measurement of $Pe_T$ comprised between [0.5, 17].

## 3.2 Meshing

The mesh was created with the open-source code SnappyHexMesh distributed with OpenFOAM, due to the complex geometry of the domain and the anticipated size for the mesh. A balance between the number of cells of the resulting mesh and the quality of the mesh must be established through multiple tests. This must be done to guarantee a small enough number of cells to minimize the high computational cost of DNS and a sufficient cell quality required for the CFD equations to converge.

Maintaining a good depiction of a real porous bed is necessary. If the cell size is large, bridges may occur between particles, as showed in Figure 11, which will result in a lower than expected porosity. To counter this without a large increase of number of cells, it was decided to decrease the cell size while approaching the particles surface.

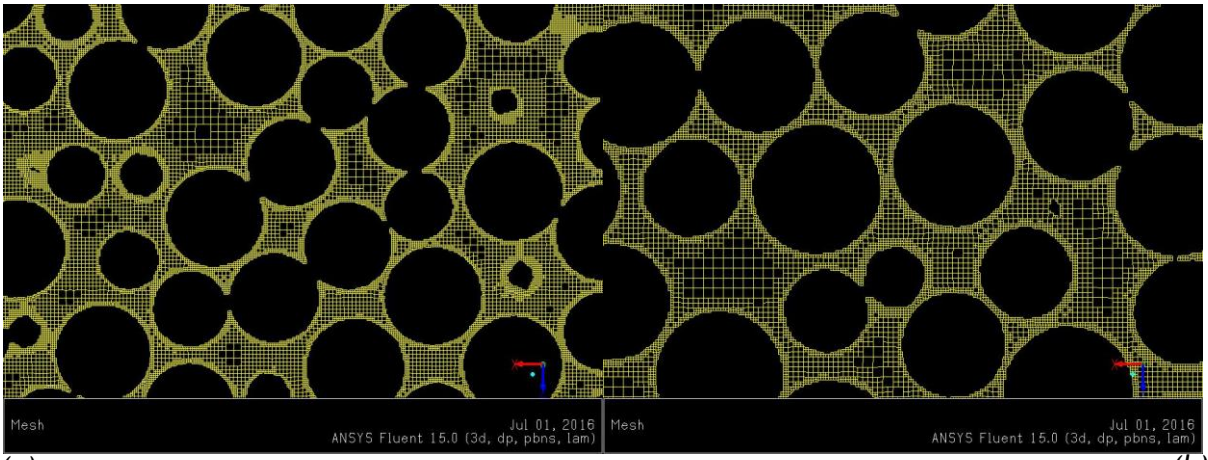


*(a)* *(b)*

*Figure 10: Influence of the number of cells on the formation of bridges, left side (a) has 18 million and the right side (b) has 120 million.*

To check if the mesh is properly snapped to the particles a comparison is made between the porosity of the mesh calculated through the CFD software and the original porosity of the DEM simulation obtained from the rendering and editing software used. Table 2 shows the results of this comparison for the same meshing conditions.

*Table 2: Average domain porosity as a function of the number of cells*

| Number of cells | | 18 million | 30 million | 60 million |
|---|---|---|---|---|
| | $\varepsilon_{DEM}$ | $\varepsilon_{CFD}$ | $\varepsilon_{CFD}$ | $\varepsilon_{CFD}$ |
| Porosity (%) | 38.68% | 37.34% | 37.53% | 37.70% |
| Deviation (%) | - | 1.34% | 1.15% | 0.98% |

From table 2, it is seen that the decrease in porosity deviation is not linearly proportional to the increase in cell number. This results in a compromise between the porosity deviation and

the number of cells and consequently the available computational power and limited number of CFD licenses.

## 3.3 Boundary Conditions and Discretization Scheme

For the 3D CFD simulation, instead of having wall boundary conditions delimitating the sides of the domain, a symmetry condition will be applied to this planes to remove the no slip condition. The inlet surface was defined by the inlet velocity of the fluid, and later, for the transverse simulation, it was separated in two, according to the Figure (11), to allow the inlet of the tracer. The outlet was defined simply as a pressure outlet with the exiting pressure being equal to the atmospheric pressure. Extra space was also added before and after the axial limits of the porous media.

For this case the pressure based solver was chosen, with the SIMPLE pressure-velocity coupling scheme, usually used for laminar flows and without the use of turbulence models. As for the spatial discretization of the convective terms of the transport equations for the passive tracer, the third-order MUSCL discretization scheme was used to potentially reduce the occurrence of numerical diffusion. (Ferziger and Perić, 2002)

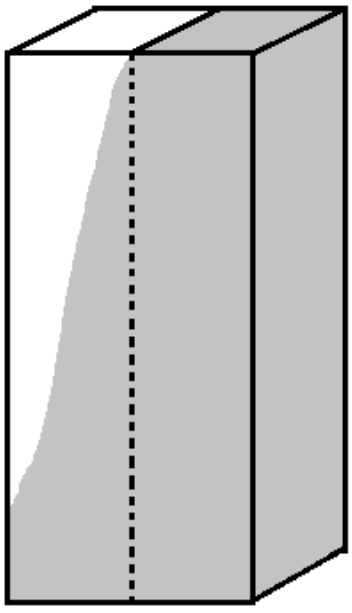

Figure 11: Sketch of the simulation domain following Han's experiment

## 3.4 Flow Validation

In order to evaluate if the generated mesh represents well the intended porous media, a comparison is made between flow simulations and the empirical model from the Ergun Equation (23), for both a fluid with an already characterized $Sc$ number (=100) by (Guedes de Carvalho, J.R.F. and Delgado, 2005) and the fluid of interest.

$$\frac{\Delta P}{L} = \frac{150\mu}{{d_p}^2}\frac{(1-\varepsilon)^2}{\varepsilon^3}U + \frac{1.75\rho}{d_p}\frac{1-\varepsilon}{\varepsilon^3}U^2 \tag{23}$$

where $\Delta P$ represents the pressure drop along the column and $L$ the length of the column.

## 3.5 Method for Obtaining the Transverse Dispersion Coefficient

As referred in Section 2.1.1, for the determination of $Pe_T$, simulations are created following the conditions specified in Han et al. (1985) for the Lateral Dispersion Experiments. Like so, after validating the flow profile for the selected fluid, the inlet surface is divided in half along the axis in which the tracer profile wishes to be obtained and tracer is introduced through one of those halves with a nominal concentration $(C = 1)$, while the other keeps an inlet of pure fluid $(C = 0)$.

The tracer mass balance equation is solved independently of the flow equations because the tracer is passive and has no impact on the flow. Results of the tracer concentration are reported along the selected direction.

Since Han's experiment is two-dimensional, the profile will be extracted by an average of the $y$ dimension (normal to the concentration-gradient at the inlet). Secondly the theoretical treatment for Han's experiment is done assuming a homogeneous porous media. However, for DNS at a small scale (below the particles diameter) simulation shows local variation of the porosity.

To solve this, it is necessary to find the characteristic dimensions of the elementary domain on which the average should be done to extract the concentration profile. The elementary domain could be a volume or a surface as shown in Figure 12.


*(a)* *(b)*

*Figure 12: Example of a Volume element (a) and a set of some surface elements (b)*

In Figure 13, the local porosity deviation along the transversal distance is plotted for the volume elements with 1 and 2 $d_p$ in length.

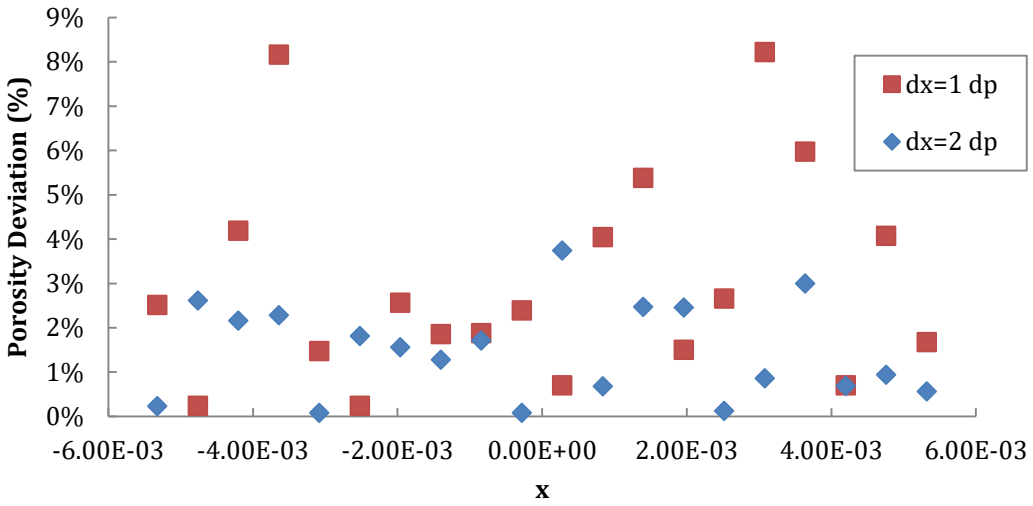


*Figure 13: Porosity deviation plotted along the transversal direction for different volume elements*

Figure 13 shows that for smaller volume elements (dx=1dp) there is a higher deviation of local porosity, which, if used, must be taken into account.

On Figure 14, 15 and 16, the breakthrough curves for the same simulation are reported using different reporting methods and comparisons are made to choose the best method.

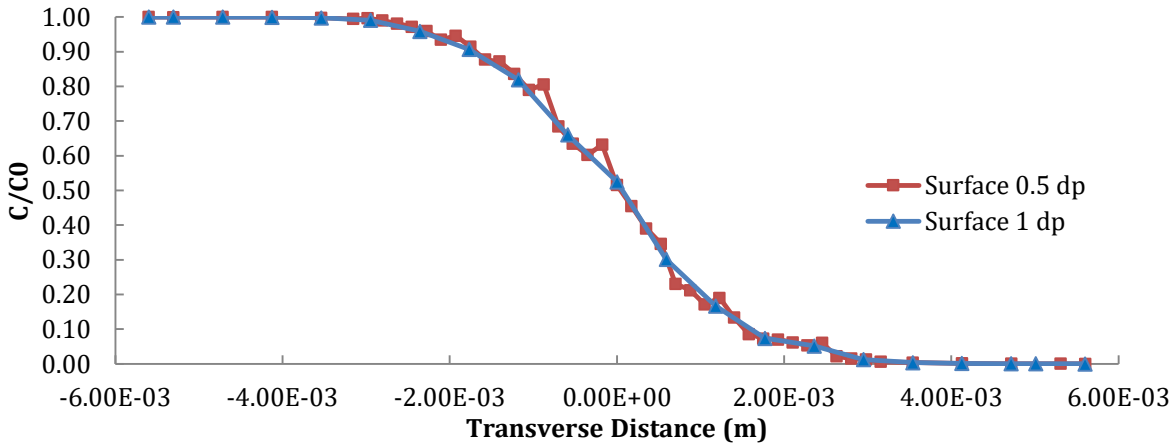


*Figure 14: Test results for surface elements with 0.5 and 1 $d_p$ of length*

From Figure 13, using a surface element with 0.5 $d_p$ results in the appearance of noise in the breakthrough curve.

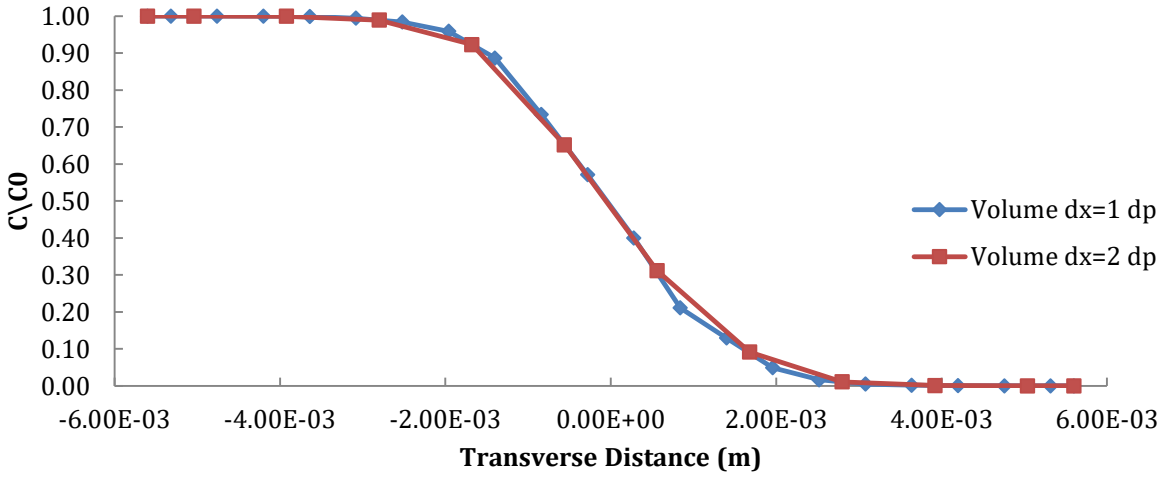


*Figure 15: Test results for volume elements with 1 and 2 $d_p$ of length*

From Figure 15, using a volume element with 2 $d_p$ in length results in a breakthrough curve with lower curvature due to the lower discretization, resulting in reports with higher than expected dispersion.

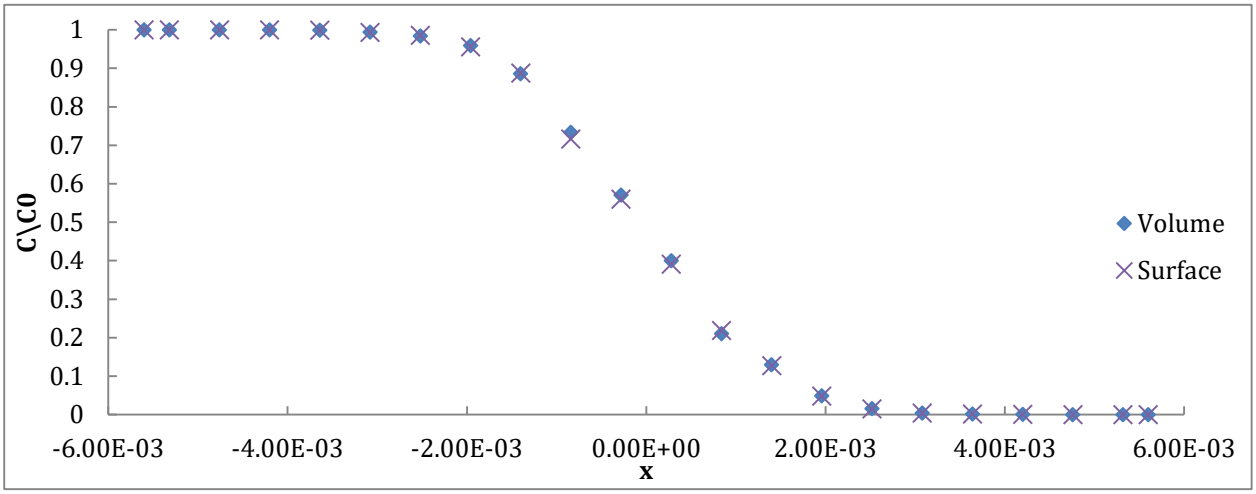


*Figure 16: Comparison of the breakthrough curves for volume and surface elements with 1 $d_p$ in length.*

The surface element with the size of one particle diameter was chosen, since the results obtained with the surface element method do not vary significantly from those obtained from the volume elements method, showed in Figure 16. Also the creation of the volume elements takes substantially more time and computational memory, however as seen in Figure 12 local porosity must be taken into account.

$Pe_T$ is determined by fitting the analytical solution, Equation (7), to the breakthrough curve by the minimization of the mean squared deviations.

The influence of the parameter $N$ in the quality of the data collected was also studied, and as shown in Figure 16, for values of $N$ of 9, 6 and 3.

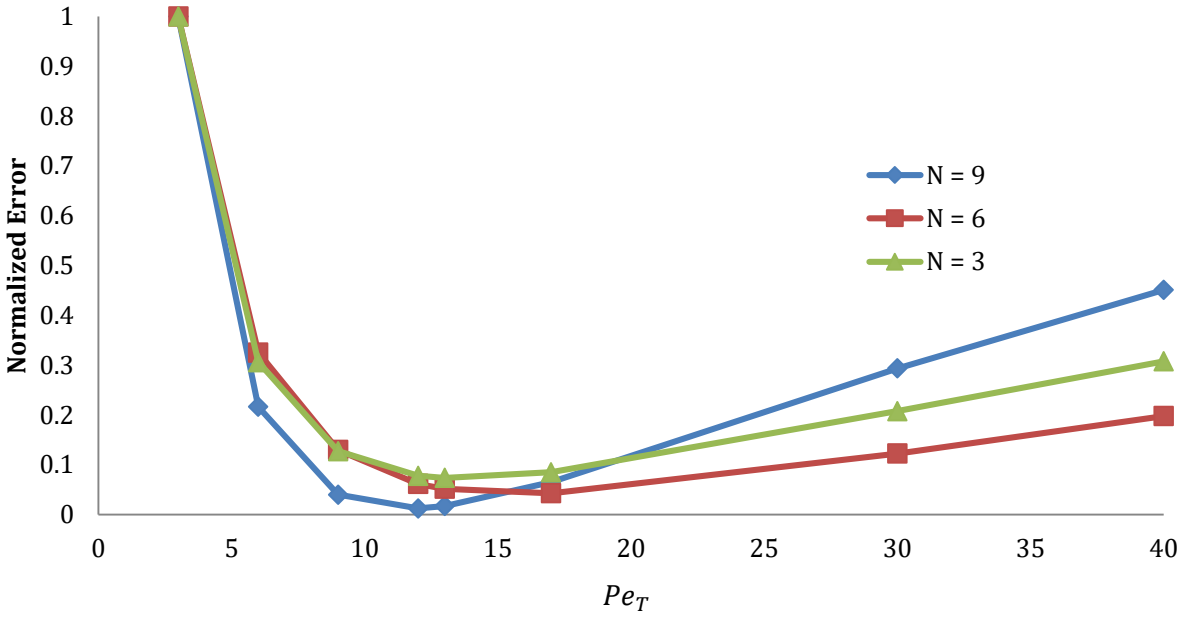


*Figure 17: Sensitivity analysis for different values of N of the minimization of the error of the fitting compared to the results*

The higher the parameter *N*, the lower the deviations between the fitting of the analytical solution and the experimental results. It also shows that for higher values of *N* there is a bigger sensitivity between the optimization function of the minimization and the $Pe_T$ and a bigger confidence in the calculated value. This analysis is important to show that these simulations could have been done with a smaller domain than the one proposed, but there would be less confidence in the obtained value for $Pe_T$.

## 3.6 Innovative Method for Obtaining the Axial Dispersion Coefficient

Following Han's et al. (1985) axial dispersion experiment, previously referred in Section 2.1.2, transient simulations would be required to obtain $Pe_L$ values.

As a response to a Dirac impulse, from the outlet of the porous media it's possible to obtain the residence time distribution (RTD) of the tracer, $E(t)$. The mean residence time $\mu_0$ and the standard deviation $\sigma^2$, represented in Figure 18, can be obtained from Equations (24) and (25) respectively.

$$\mu_0 = \int_0^\infty E(t)t\,dt \tag{24}$$

$$\sigma^2 = 2\int_0^\infty E(t)\,t^2 dt \tag{25}$$

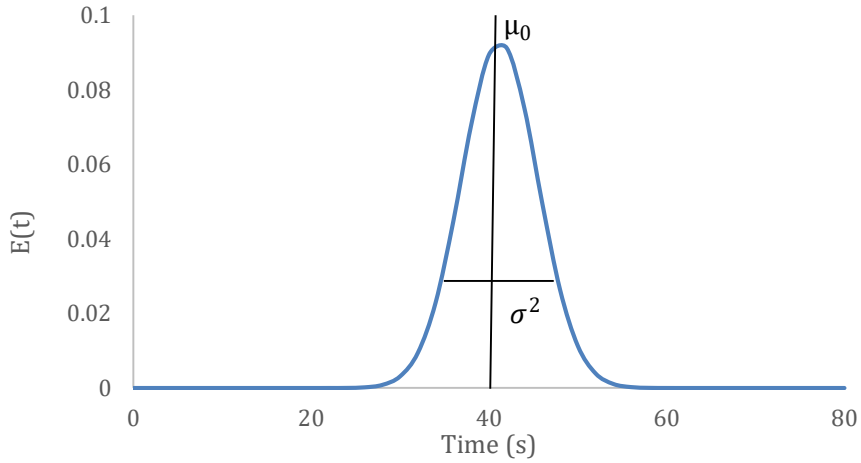


*Figure 18: Example of an RTD response*

Assuming that the present case could be modeled as a cascade of CSTR, the equivalent number of CSTR ($J$) can be obtained from Equation (26)

$$J = \frac{{\mu_0}^2}{\sigma^2} \tag{26}$$

Villermaux (1993) has shown that for a $J > 100$, the number of CSTRs can be related to the equivalent Péclet number, $Pe_{eq}$

$$Pe_{eq} = 2(J - 1) \tag{27}$$

This Péclet number is defined relatively to the total length of the domain.

$$Pe_{eq} = \frac{uL}{D_L} \tag{28}$$

Finally, as referred in Section 2.1.2, the basis to Han's longitudinal experiment is to eliminate the influence of transversal dispersion, if so then the $Pe_{eq}$ obtained from the DTR only possesses the contribution of the longitudinal dispersion, allowing the determination of $Pe_L$ from Equation (30).

$$Pe_L = Pe_{eq}\frac{d_p}{L} \tag{30}$$

As running these transient simulations would be very time consuming, an alternative method in steady-state approach is proposed to mitigate these limitations by using the moment transport method to calculate the moments $M1$ and $M2$ experimented in the flow.

$M1$ and $M2$ are transported as scalars in the CFD simulations and source terms are imposed via a user defined function (UDF), which is shown in Annex 1.

By mass-weighted average of $M1$ and $M2$ at the outlet of the domain, $\mu_0$ and $\sigma^2 + {\mu_0}^2$ can respectively be calculated.

# 4 2D Axisymmetric Simulations

## 4.1 Porosity profile determination

To study the impact of the near wall channeling effects on the value of the global dispersion coefficient $Pe_{eq}$, 2D axisymmetric simulations of an equivalent packed column were created, as opposing the case with a constant porosity profile. As such, the correct characterization of the porosity profile is an essential step of this work. As referred in Section 2.2, experimental results will be obtained from CAT scans of a real packed bed and will be compared and fitted to the correlation derived from the Giese experiments (Augier 2008) described in Equation (31). Finally, Equation (31) will also be used to model the porous media of the 2D axisymmetric simulations of an equivalent packed column.

$$\varepsilon = A + B \times \cos\left(\frac{2\pi x}{d_p}\right) e^{\frac{-x}{Cd_p}} + De^{\frac{-x}{Ed_p}} \tag{31}$$

In Augier 2008 the proposed values for the constant parameters are $A = 0.32$, $B = 0.35$, $C = 1.061$, $D = 0.21$ and $E = 1.88$.

## 4.2 Computational domain

The simulations for Section 4 for will be performed using a 2D axisymmetric model, with the axis of symmetry along the length of the column, with a size 1.2 meters in length and 1 centimeter in the radial direction, this domain represents a cylindrical column of the same dimensions with a constant face size in the axial direction and a continuously decreasing face size in the transverse direction, smaller the closer it is to the wall, to account for the increasing variation of the porosity and flow due to the near-wall porosity effects, as represented in Figure 19.

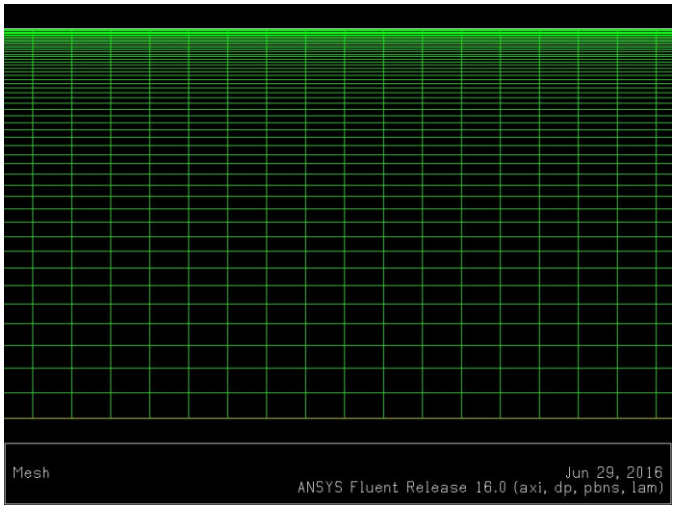


*Figure 19: Zoom in on the mesh used for the 2D simulations*

## 4.3 Flow and Transport Modelling

This 2D case will be solved using an axisymmetric model and by setting a porous zone in the whole domain. The flow equations will be resolved with the same discretization schemes as the previous simulations.

The porous zone characteristics will be set with the use of UDFs taking into special detail:

- the definition of the porosity, comparing the results from the profiles obtained from the CAT scans or the values proposed by Augier.
- the anisotropic diffusivity in which the $\mathrm{Pe_T}$ and $\mathrm{Pe_L}$ will be tested for the correlations of GDC and Gunn with the value of $\mathrm{Pe_m}$ as a function of the mean column velocity or as a function of the local velocity.
- pressure-drop model, in which a variation of the laminar Navier-Stokes equations for porous media will be used, the model of Brinkman-Forcheimer.

From the model of Brinkman-Forcheimer two variables are obtained for the representation of the liquid/solid interactions: the permeability $K$ and the non-Darcy term $\beta$ which are calculated from the Ergun law.

$$K = \frac{\varepsilon^3 d_p^2}{150(1-\varepsilon)^2} \tag{32}$$

$$\beta = 1.75\frac{1-\varepsilon}{\varepsilon^3\, d_p} \tag{33}$$

The method used to determine the dispersion coefficient in the 2D axisymmetric simulations will be the same as the one used for the 3D longitudinal simulations and described in Section 3.6. However, since these simulations only take into account the global scale dispersion the results will be presented as the $J$ for different values of $Pe_m$.

# 5 Results

## 5.1 Flow Validation

The flow field obtained from the CFD simulations will be validated by comparing the pressure drop obtained with the pressure drop predicted by the Ergun equation, Equation (23).

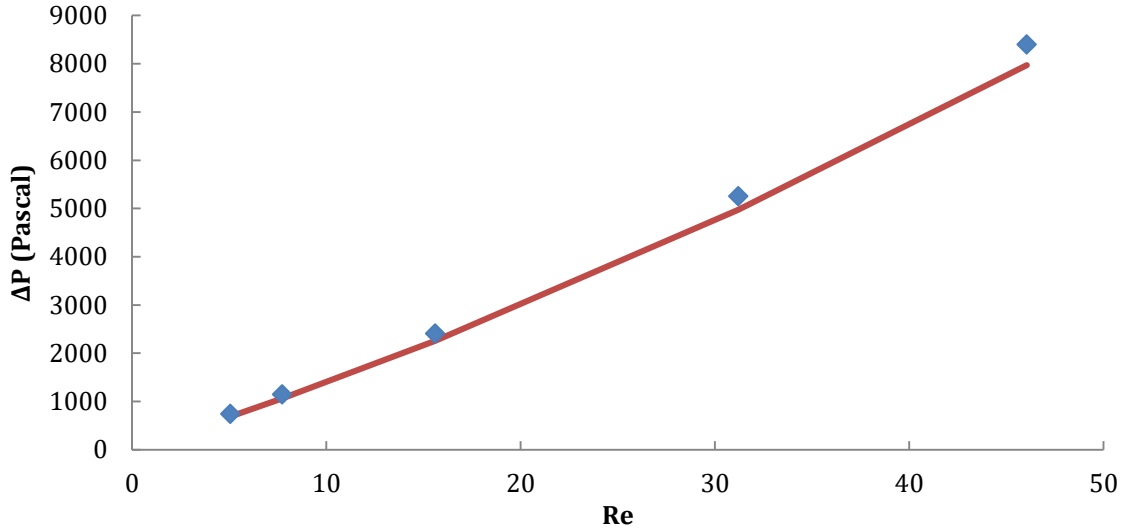


*Figure 20: Comparison of the ΔP previewed from Ergun and the obtained results for* $Sc = 100$

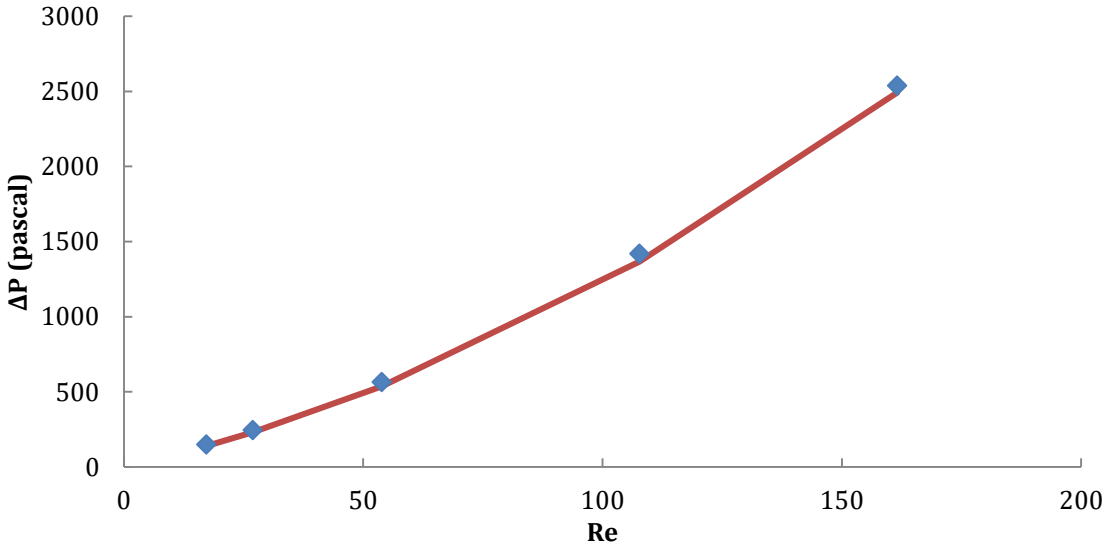


*Figure 21: Comparison of the ΔP previewed from Ergun and the obtained results for* $Sc = 29$

Figures 20 and 21 show that there is a good agreement between the CFD results and the Ergun equation with an average deviation of 7% for $Sc = 100$ and 5% for $Sc = 29$. All the results obtained for the flow validation are present in table 3.

*Table 3: Collection of the pressure drop for both fluids at different velocities*

| *Sc* | *u* | *ΔP* | *ΔP Ergun* | *Deviation* |
|---|---|---|---|---|
| | 0.0032 | 148 | 139 | 6% |
| | 0.0050 | 244 | 231 | 6% |
| ***29*** | 0.0100 | 564 | 536 | 5% |
| | 0.0200 | 1420 | 1366 | 4% |
| | 0.0300 | 2538 | 2492 | 2% |
| | 0.0034 | 741 | 683 | 8% |
| | 0.0052 | 1146 | 1064 | 6% |
| ***100*** | 0.0105 | 2408 | 2262 | 6% |
| | 0.0210 | 5251 | 4972 | 6% |
| | 0.0310 | 8398 | 7970 | 5% |

## 5.2 New Data for Transverse Dispersion coefficients

The obtained data points for the $Pe_T$ are shown in Figures 22 and 23. in Figures 20 and 21, the proposed correlations are also plotted for each respective fluid to verify if the results are well predicted by any correlation.

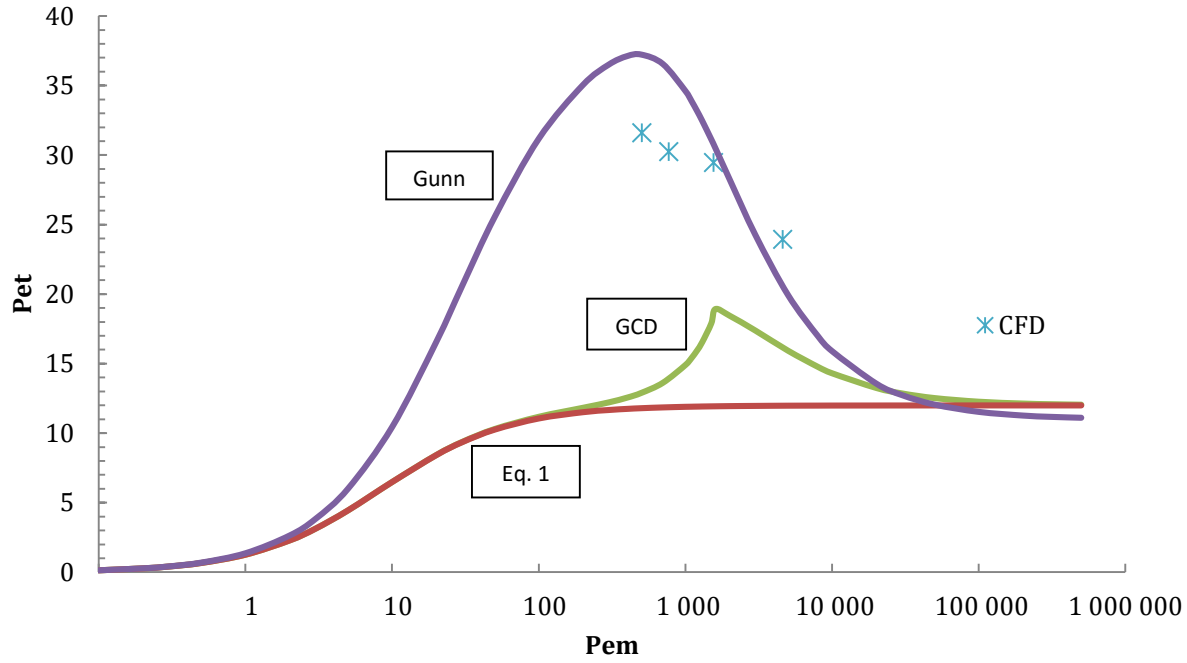


*Figure 22: Comparison of the experimental results of $Pe_T$ with the correlations for Sc=100*

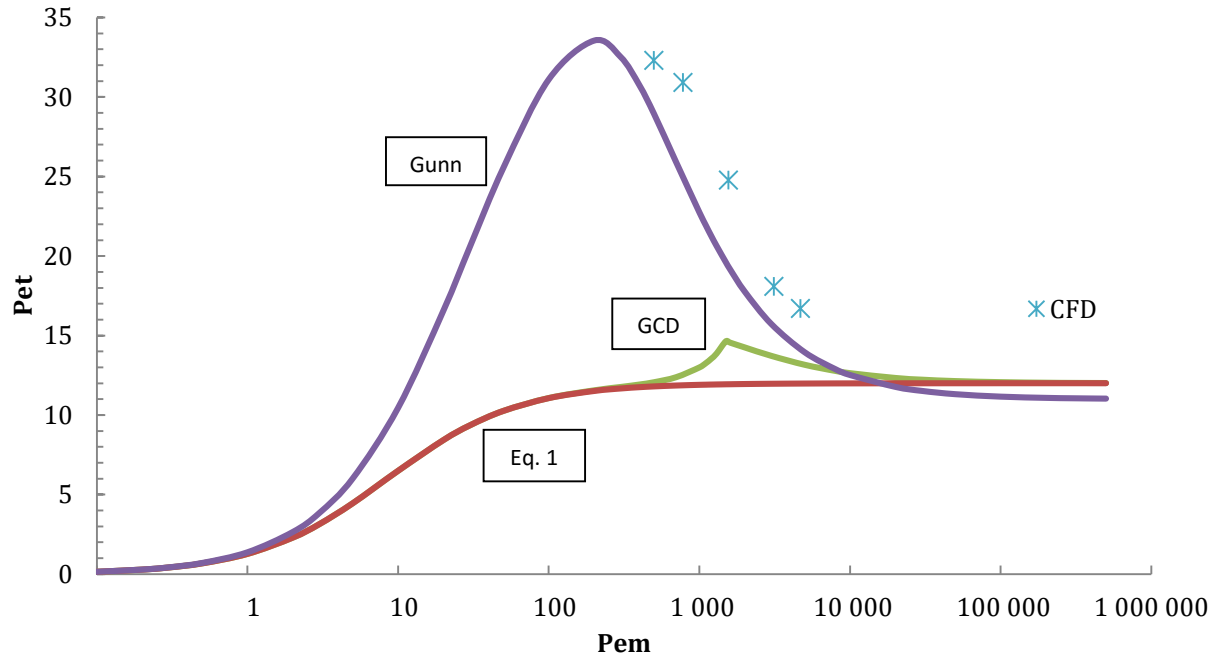


*Figure 23: Comparison of the experimental results of $Pe_T$ with the correlations for $Sc = 29$*

Figures 22 and 23 show that the experimental points show a good agreement with the correlation proposed by Gunn (1969). However, the obtained $Pe_T$ results are outside the values proposed in this work, in the Section 3.1.2 ($Pe_T \in [0.5, 17]$), as confirmed from Table 4. The insufficient domain size and chosen data extraction section are the reasons for the deviations between the fitting of the experimental results and the correlation of Gunn (1969).

The experimental result for the fluid with $Sc = 100$ and $Pe_m = 3119$ was left out of the final results for the uncertainty of the correct convergence of the solution.

*Table 4: Collection of the $Pe_T$ results for both fluids and different velocities*

| Sc | Re (=f(u)) | U | $Pe_m$ | $Pe_T$ fitted on the DNS results | $Pe_T$ from the GCD correlation | $Pe_T$ from the Gunn correlation |
|---|---|---|---|---|---|---|
| | 17 | 0.0032 | 500 | 32.31 | 12.06 | 28.94 |
| | 27 | 0.0050 | 781 | 30.92 | 12.53 | 24.92 |
| **29** | 54 | 0.0100 | 1562 | 24.78 | 14.92 | 19.32 |
| | 108 | 0.0200 | 3123 | 18.09 | 13.68 | 15.32 |
| | 162 | 0.0300 | 4685 | 16.69 | 13.23 | 14.13 |
| | 5 | 0.0034 | 505 | 31.60 | 12.92 | 37.22 |
| | 8 | 0.0052 | 772 | 30.24 | 13.91 | 36.14 |
| **100** | 16 | 0.0105 | 1560 | 29.45 | 18.36 | 30.75 |
| | 31 | 0.0210 | 3119 | - | 17.28 | 23.88 |
| | 46 | 0.0310 | 4605 | 23.93 | 16.17 | 20.56 |

## 5.3 New Data for Axial Dispersion coefficients

The results obtained for the proposed method of obtaining the axial dispersion coefficients described in Section 3.6 are shown in Table 5.

*Table 5: Experimental results for the $Pe_L$ using the initial methodology*

| $Sc$ | 100 | | 29 | |
|---|---|---|---|---|
| $Pe_m$ | J | $Pe_L$ | J | $Pe_L$ |
| **523** | 61 | 1.190 | 62 | 1.220 |
| **817** | 58 | 1.150 | 61 | 1.200 |
| **1633** | 54 | 1.050 | 59 | 1.170 |
| **3267** | 50 | 0.981 | 23 | 4.340 |
| **4900** | 47 | 0.927 | 41 | 0.793 |

However, as shown in Table 5, neither set of points has a value of *J* bigger than 100, indicating that Equation (27) may not be a valid approximation. To overcome this, the moments $M1$ and $M2$ must be calculated from the analytical solution proposed in Section 2.1.2.1, Equation (12).

The values for $Pe_L$ will be obtained by fitting the second moment ($\sigma^2 + \mu_0{}^2$) of Equation 12 to the value of $M2$ obtained from the experimental results.

Figures 24 and 25 show the obtained data points for the $Pe_L$ for $Sc = 100$ and for $Sc = 29$, respectively. In the same figures the proposed correlations are also plotted for each fluid to verify if the results follow any correlation.

Figures 22 and 23 show the obtained data points for the $Pe_L$. In the same figures the proposed correlations are also plotted for each fluid to verify if the results follow any correlation.

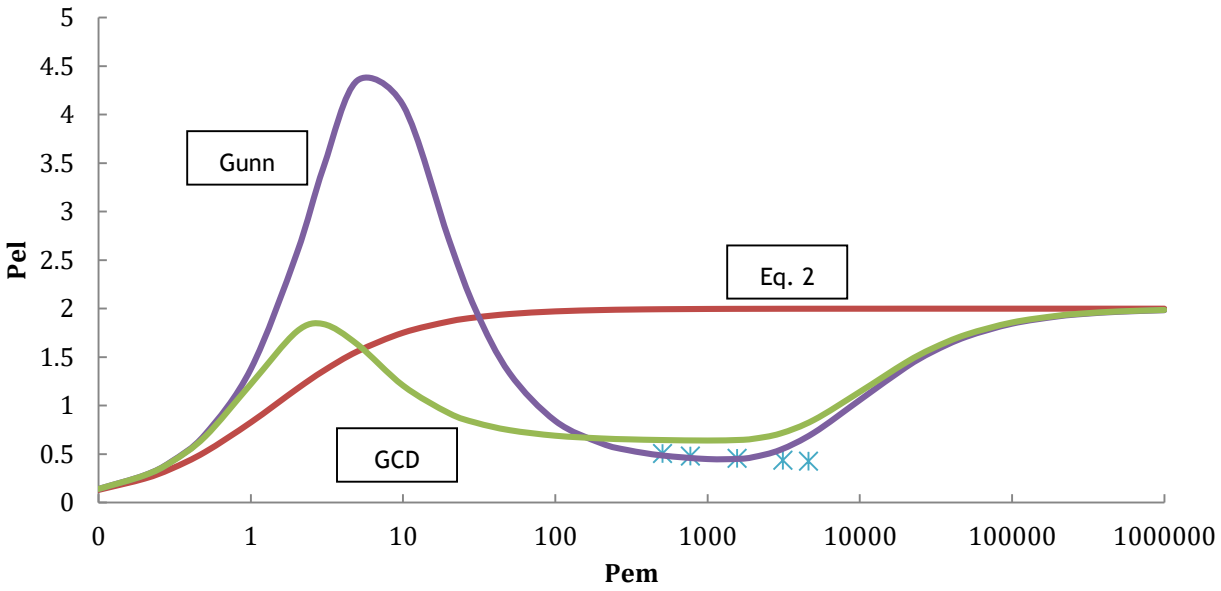


*Figure 24: Comparison of the experimental results of $Pe_L$ with the correlations for $Sc = 100$*

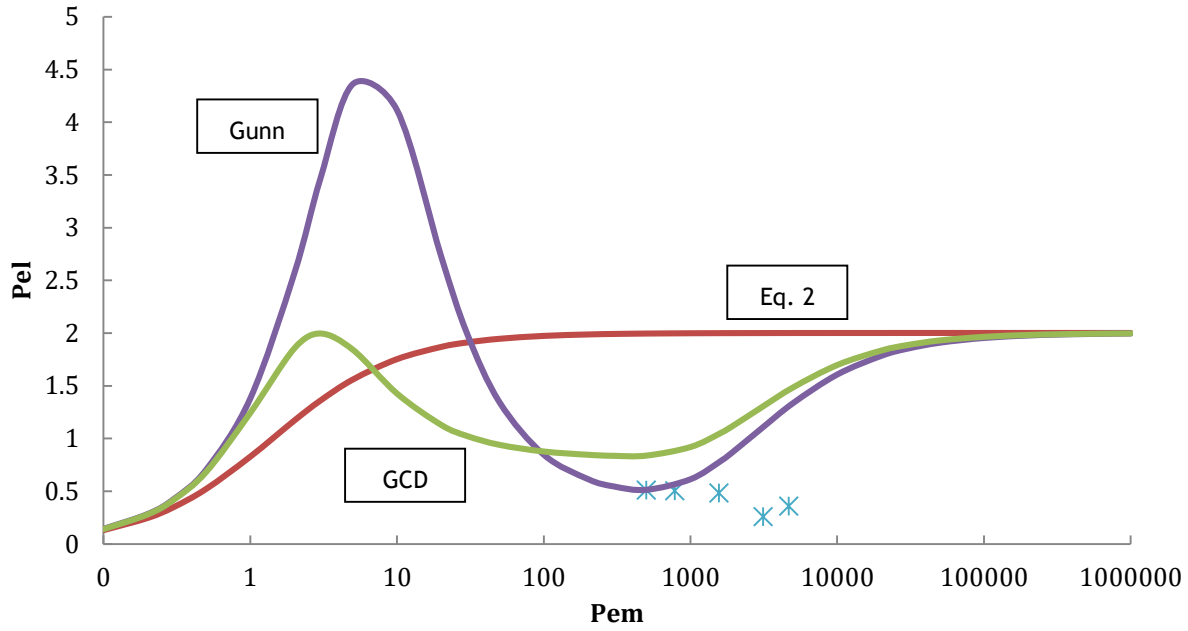


*Figure 25: Comparison of the experimental results of $Pe_L$ with the correlations for $Sc = 29$*

For the fluid with $Sc = 100$ and for $Pe_m \leq 1560$, the values of $Pe_L$ are well described by the correlation of Gunn (1969). For $Pe_m > 1560$, the experimental values show a lower $Pe_L$ than predicted by Gunn (1969), and therefore bigger axial dispersion.

For $Sc = 29$, Figure 25, similar behavior is observed. For $Pe_m \leq 781$ $Pe_L$ is well described by the correlation of Gunn (1969). For $Pe_m > 781$, the experimental values show a lower $Pe_L$ than expected, this may be a result of the increase of the Reynolds number to a possible non-laminar regime, as shown in Table 4.

The results for $Pe_L$ of both fluids are presented in Table 6.

*Table 6: Experimental results for the $Pe_L$ obtained by fitting the second moment of Equation 12 to M2*

| $Sc = 100$ | | $Sc = 29$ | |
|---|---|---|---|
| $Pe_m$ | $Pe_L$ | $Pe_m$ | $Pe_L$ |
| 505 | 0.51 | 500 | 0.51 |
| 772 | 0.48 | 781 | 0.50 |
| 1560 | 0.46 | 1562 | 0.49 |
| 3119 | 0.44 | 3123 | 0.26 |
| 4605 | 0.43 | 4685 | 0.36 |

## 5.4 Porosity profile

For the determination of the porosity profile of the real packed bed, two Matlab codes were developed. A first one for plotting the averaged accumulated porosity *vs.* the number of scans, images obtained as a result of a Computational Axial Tomography, and was used to determine the minimum number of images necessary to obtain a constant porosity average. The second one uses the results obtained from the first one, to plot the porosity profile along the radial direction so it can be fitted by Giese experimental expression, Equation (31), and used in the flow simulations.

Figure 26 shows the number of images necessary to obtain a constant averaged porosity, necessary to later obtain a reliable porosity profile. The values reported in this figure were obtained from the use of Matlab code, available in Annex 2.

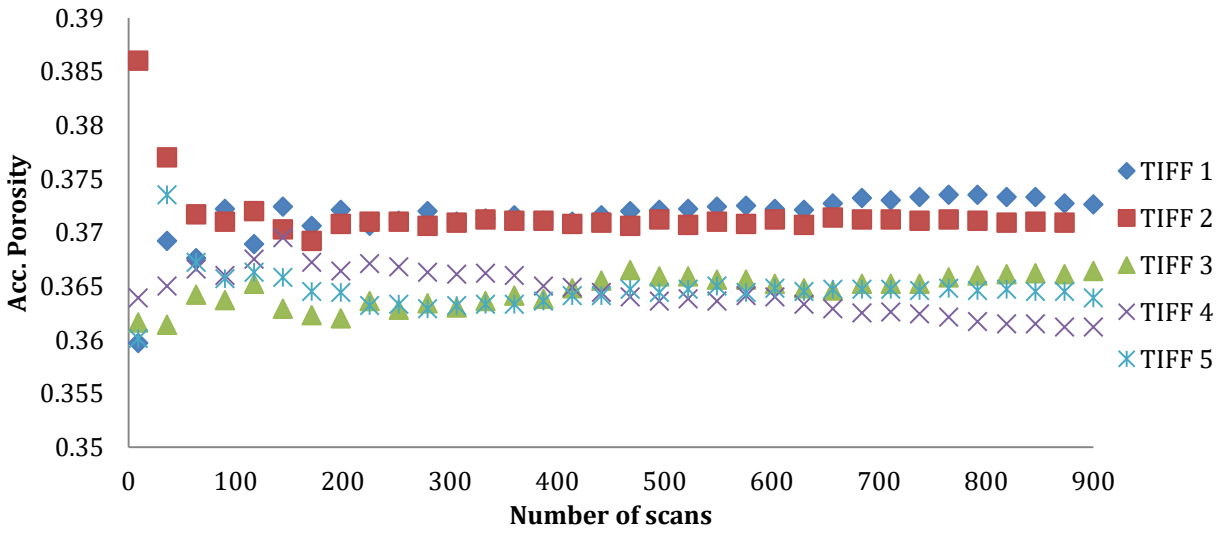


*Figure 26: Plot of accumulated porosity as a function of processed images by image stack*

Most stacks seem to maintain a constant value of porosity using 500+ images. However, the porosity of the image stacks TIFF 1 and TIFF 4 does not converge with the maximum number of images, and so will be disregarded from further process.

An averaged porosity profile was made from the remaining samples and was fitted based on the Giese mathematical correlation, Equation (31), as showed in Figure 27, obtaining the intended fitting parameters displayed in Table 7.

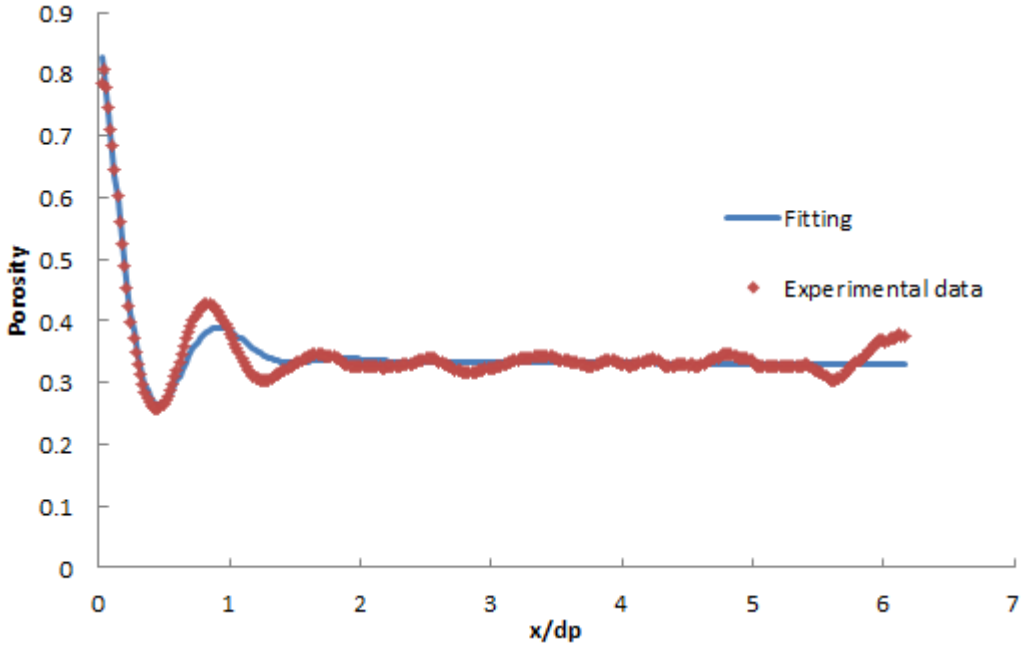


*Figure 27: Averaged porosity profile obtained from the CAT scans and the fitting profile based on the Giese experiments*

In Figure 27, the experimental results show an increase in porosity near the center of the column, which as disregarded in the fitting and may be caused by the lower analysis area near the center. The used mathematical correlation does not show a good fitting around $x/d_p = 1$ and as such a different correlation should be used to obtain better results.

*Table 7: Fitting parameters for the porosity profile obtained from the CAT scans*

| A | B | C | D | E |
|---|---|---|---|---|
| 0.330 | 0.413 | 0.366 | 0.111 | 0.634 |

The obtained porosity profile is compared to the one proposed by Augier et al. (2010), in Figure 27. The porosity profile obtained from the CAT scans shows significantly less near-wall channeling effects that the one proposed by Augier, evident by the more flattened profile.

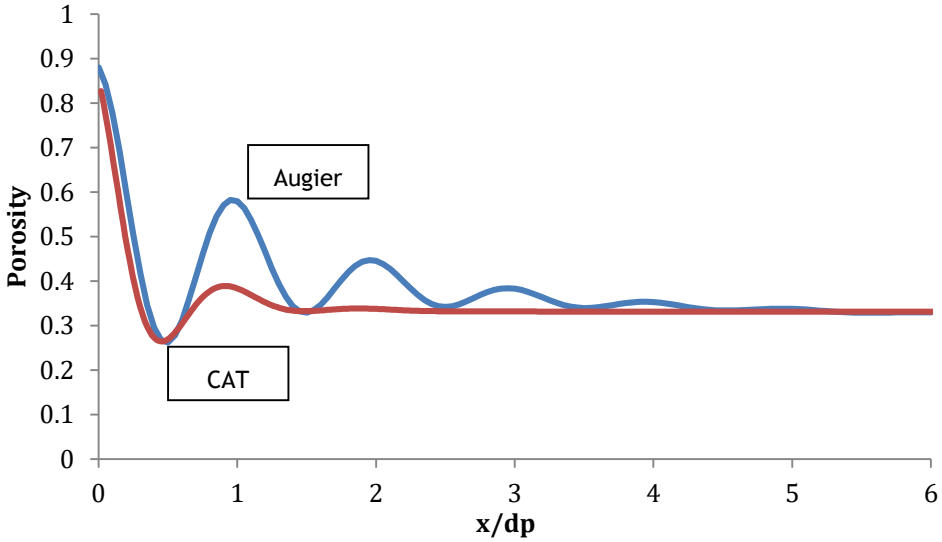


*Figure 28: Comparison of the used porosity profiles from Augier and the one obtained from the processing and fitting of the CAT scans*

## 5.5 Simulation of the equivalent porous media (RTD comparison)

Results for the 2D equivalent porous media simulations are plotted in Figures 28, 29, 30, 31 and 32. This figures will represent the number of equivalent CSTR, $J$, vs $Pe_m$ for different conditions.

Figure 28 shows the results with a constant porosity profile and with constant Péclet numbers ($Pe_T = 11$ and $Pe_L = 2$) and will be used as a reference.

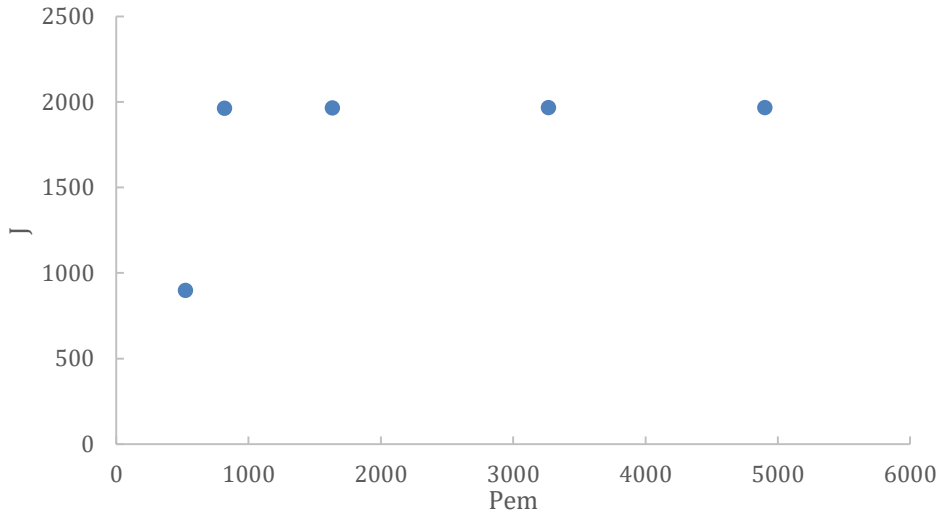


*Figure 29: Reference results for $\varepsilon = 0.37$, $Pe_T = 11$ and $Pe_L = 2$*

From Figure 29, the results show that for a constant velocity and constant Péclet numbers the column shows a behavior that can be described as plug-flow, an increase in $Pe_m$ makes $J$ tend to a constant value.

Figure 30 and 31 show comparisons made between the results obtained for a $Pe_m$ as a function of constant global velocity and for a function of local velocity. In Figure 30, results are compared using the porosity profile proposed by Augier et al. (2010) and with the anisotropic diffusivity determined with the GCD correlations.

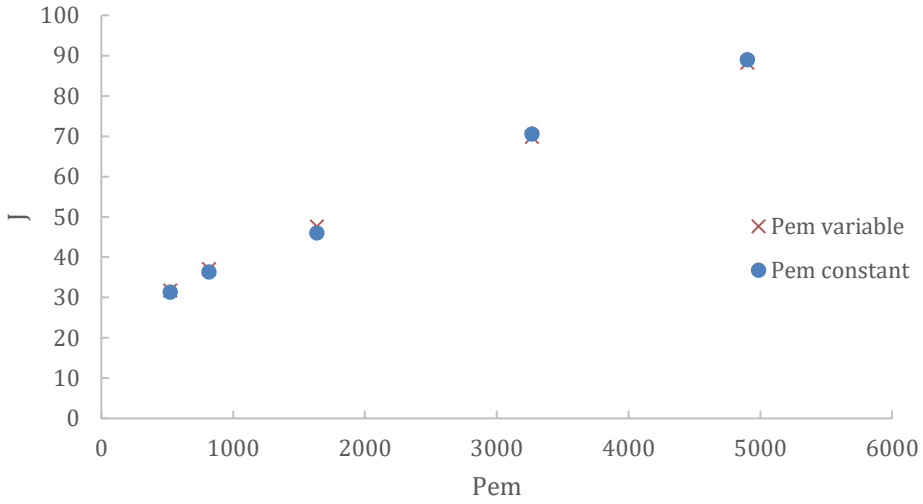


*Figure 30: Comparison of the influence of $Pe_m$ as a function of global and local velocity, with the porosity profile proposed by Augier and the dispersion correlations by GCD.*

In Figure 31, results are compared using the porosity profile proposed by Augier et al. (2010) and with the anisotropic diffusivity determined with the Gunn correlations.

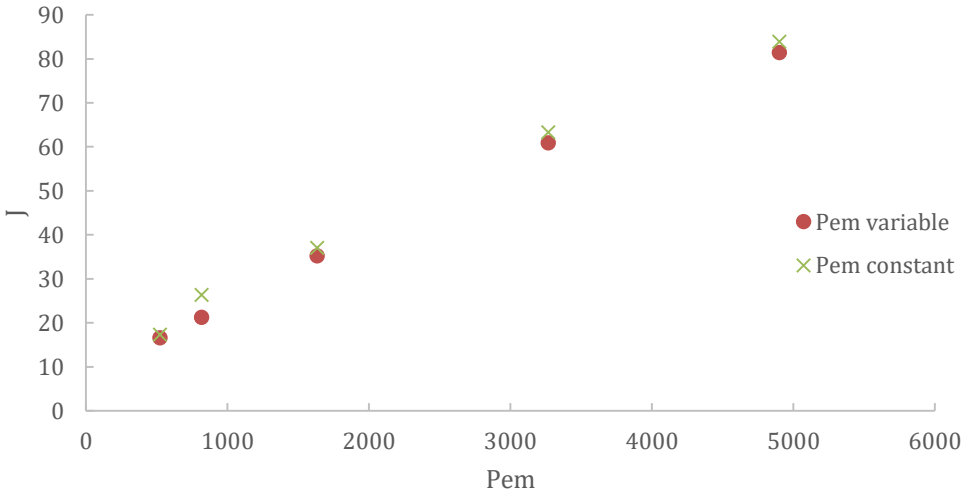


*Figure 31: Comparison of the influence of $\boldsymbol{Pe_m}$ as a function of global and local velocity, with the porosity profile proposed by Augier and the dispersion correlations by Gunn.*

Simulations were made using the dispersion coefficients from Gunn and GCD with $Pe_m$ as a function of local velocity or global velocity. According to the results in Figures 30 and 31 there is little influence of the local velocity for the calculation of $J$, compared with the use of the global velocity.

Figure 31 compares the results of $J$ using the two different correlations for the anisotropic diffusivity, GCD and Gunn, with a $\mathrm{Pe_m}$ as a function of the local velocity.

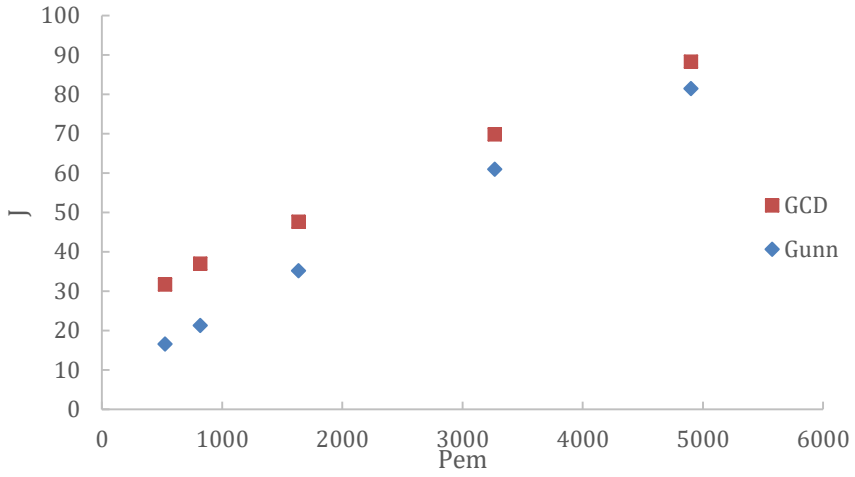


*Figure 32: Comparison of the results of the correlations from Gunn and GDC*

Comparing the outcome for the correlations of Gunn and GCD for the transversal and axial dispersion, unexpected results are encountered. In Figure 32, results from GCD show more plug-flow behavior than the results from Gunn, which have a higher $Pe_T$ and therefore lower transversal dispersion.

A possible explanation resides in the lower transversal dispersion from the correlations of Gunn. The near-wall channeling effects promotes velocity and concentration gradients in the axial direction near the walls, however for a low diffusivity mixing will not be present. If so, younger molecules will be found near the wall, due to the higher velocity, and the older ones will stay in the center of the column. With just the influence of the velocity profile the overall dispersion will be bigger.

For the coefficient proposed by GCD the transversal dispersion promotes the mixing and smoothing of the molecules' age in the transversal direction, resulting in a more uniform axial dispersion.

Figure 32 compares the results obtained from the use of the porosity profile from Augier and the one obtained from the CAT scans.

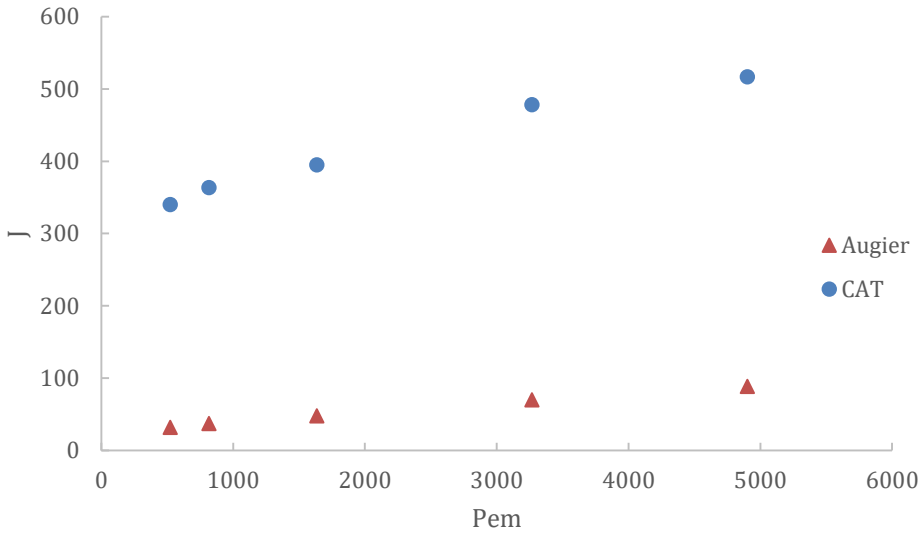


*Figure 33: Comparison of the results with the porosity profile from Augier and the porosity profile obtained from the CAT scans*

Figure 32 shows that the porosity model developed from the porosity profile obtained from the CAT scans has a more plug-flow like behavior than the profile proposed by Augier et al. (2010). Recalling Figure 27, the porosity profile of Augier et al. (2010) has more near wall channeling effects than the profile obtained from the CAT scans, these effects result in a decrease of the number of CSTR.

Finally, in Table 8 all the results obtained from the 2D axisymmetric simulation of the equivalent porous media are shown.

*Table 8: Compilation of the results for the 2D simulations*

| | $\boldsymbol{\varepsilon = 37\%}$ | **AUGIER** | | | | **CAT** |
|---|---|---|---|---|---|---|
| $\boldsymbol{Pe_m}$ | $Pe_T = 11$ $Pe_L = 2$ | GCD | | Gunn | | GCD |
| | | $Pe_m$=f(u) | $\boldsymbol{Pe_m}$=f(const) | $Pe_m$=f(u) | $\boldsymbol{Pe_m}$=f(const) | $Pe_m$=f(u) |
| | J | J | J | J | J | J |
| **523** | 898 | 32 | 31 | 16 | 17 | 340 |
| **817** | 1962 | 37 | 36 | 21 | 26 | 364 |
| **1633** | 1964 | 48 | 46 | 35 | 37 | 395 |
| **3267** | 1966 | 70 | 71 | 61 | 63 | 479 |
| **4900** | 1966 | 88 | 89 | 81 | 84 | 517 |

# 6 Conclusions

## 6.1 Accomplished Objectives

In this work a 3D model of the flow and tracer dispersion in a packed bed was developed, which was able to accurately describe the flow through a packed bed. A good agreement with correlations of results for $Pe_T$ are obtained for Xylene at 170 ºC. However more accurate results could have been obtained if a bigger domain than the one proposed as used. For the valid data, the results indicated that the fluid with $Sc = 29$ is well represented by the correlation of Gunn (1969).

Longitudinal dispersion values where obtained for the intended conditions, but since $J$ is smaller than 100 in all cases, $Pe_L$ values were obtained by fitting the analytical solution to the experimental results. The resulting $Pe_L$ show a good agreement with the correlation of Gunn (1969). However, for $Re > 46$, values for $Pe_L$ show a deviation from the correlation which may be caused by the presence of a non-laminar regime.

The influence of the parameter $N$ in the calculation of the $Z$ of the analysis section was studied on Equation (17) and was concluded that for lower values of *N* the resulting data would have a bigger overall error from the deviation between the reported data and fitting points and less precision for the correct value of the $Pe_T$. Resulting in a lower confidence of the reported data at such distance in the longitudinal direction.

CAT images proved to be a viable method to characterize the interior of a real packed column. The porosity profile has been fitted to Giese mathematical correlations, so it can be used for future simulations. The fitting, however didn't properly characterize the data obtained and another fitting expression must be tested.

A 2D axisymmetric model of the equivalent porous media is successfully used to study the near wall channeling effects of both the porosity profile suggested by Augier and the one obtained from the CAT scans. The profile obtained from the CAT scans is smoother than the one proposed by Augier, and as such, the resulting equivalent packed bed has more of a plug-flow behavior. Using the correlations from Gunn and GCD to determine the influence of the local velocity in the $Pe_m$ and in the $Pe_{eq}$, shows that for the present conditions, this influence is negligible.

## 6.2 Limitations and Future Work

The major limitation of this work revolves around the generation of an appropriate numerical mesh for the CFD simulations. Numerical diffusion can be reduced by using higher order discretization schemes or decreasing the cell size. In the present work, domains with a cell number up to 60 million cells have been generated, CFD simulations were run with the highest order discretization scheme and numerical dispersion was eliminated for the studied velocities. The DEM code used, Grains3D has difficulty in generating domains bigger than the one used in this work, limiting the possibility of obtaining better results for $Pe_T$. The chosen meshing software, OpenFoam, has also been unsuccessful in exporting bigger domains to the CFD software due to memory issues.

As future work, a different meshing scheme can be explored, such as, overall smaller cell size instead of the surface proximity approach. Instead of the current method, the tracking of a high number of flow passive particles, for conditions which the molecular diffusion can be negligible can be studied. Or as a final alternative, consider the possibility of using exclusively OpenFoam code to make the domain and run the simulation. Since it has no licensing limit and there is no need to export large amounts of information to another software.

For the CAT scans processing, a better fitting expression must be tested other than the Giese mathematical correlation to obtain a more effective fitting.

For the determination of the axial dispersion coefficients with the 3D simulations, transient simulations proposed by Han (1985) could be attempted.

## 6.3 Final Appreciation

On a personal note, I found this task worth pursuing, knowledge of the dispersion mechanics and how they are changed by different physical circumstances, as the temperature and used packing, is very important for all processes that involve reaction or separation through packed beds.

This work has a lot of potential for future investigation, as many options for further development were left open at the end of this thesis.

# 7 References

Augier, F., Idoux, F., Delenne, J.Y., 2010. Numerical simulations of transfer and transport properties inside packed beds of spherical particles. Chemical Engineering Science 65 (3), 1055–1064. 10.1016/j.ces.2009.09.059.

Baker, J., 2011. CFD simulation of flow through packed beds using the finite volume technique.

Coelho, M.A.N., Guedes de Carvalho, J.R.F., 1988. Transverse dispersion in granular beds. Part 1. Mass transfer from a wall and the dispersion coefficient in packed beds. Chemical Engineering Research and Design 66.

Ferziger, J.H., Perić, M., 2002. Computational Methods for Fluid Dynamics. Springer Berlin Heidelberg, Berlin, Heidelberg.

Guedes de Carvalho, J.R.F., Delgado, J., 2005. Overall map and correlation of dispersion data for flow through granular packed beds. Chemical Engineering Science 60 (2), 365–375. 10.1016/j.ces.2004.07.121.

Gunn, D.J., 1986. Axial and Radial dispersion on fixed beds. Chemical Engineering Science 42 (2), 363–373.

Han, N.-W., Bhakta, J., Carbonell, R.G., 1985. Longitudinal and lateral dispersion in packed beds: Effect of column length and particle size distribution. AIChE J. 31 (2), 277–288. 10.1002/aic.690310215.

Villermaux, J., 1993. Génie de la réaction chimique: Conception et fonctionnement des réacteurs, 2nd ed. Tec & Doc Lavoisier, Paris, Londres, New York.

Wachs, A., Girolami, L., Vinay, G., Ferrer, G., 2012. Grains3D, a flexible DEM approach for particles of arbitrary convex shape — Part I: Numerical model and validations. Powder Technology 224, 374–389. 10.1016/j.powtec.2012.03.023.

# Annex 1

In this annex, it shows the C code used to determine the moments $M1$ and $M2$ for the transport of the moments method, implemented as a UDF in the CFD software.

```
/*udf pour le calculs des moments*/
DEFINE_SOURCE(sourcem1,c,t,dS,eqn)
{
real source;
source = 1*C_R(c,t);
return source;
 }

  DEFINE_SOURCE(sourcem2,c,t,dS,eqn)
 {
real source;
source = 2*C_UDSI(c,t,0)*C_R(c,t);
return source;
 }
```

# Annex 2

This Annex shows the codes used in Matlab for the determination of the radial porosity profile. Function porovsn_matrixm return the plot of Accumulated porosity versus number of images and Function porovsr_matrixm return the plot of porosity versus radial distance.

```
function porovsn_matrixm(nfile,step,lim,nim)
% Calculate and plot the accumulated porosity vs number of images

% nfile - Numerical identidy for the TIFF file to analyze
% step  - Interval between two consecutive points in the plot
% lim   -  Minimum number of images required for the "cut" method to work
%          properly. Recommended value of 40, lower values may cause an
%          incomplete scan.
% nim   -  Number of images to be analised, must be lower or equal to the
%          maximum number of images in the TIFF stack

% Identify TIFF stack file from directory
list= dir('*.tif');
tiffile=list(nfile).name;

info=imfinfo(tiffile);
np = nim/step;
% First point starts at lim images
np =round(np)-lim;

% Define n vector as number of points/images
n=zeros(np,1);
n(1)=lim;
for i=2 : np
   n(i)= n(i-1)+step;
   if n(np)~= nim
      n(np)=nim;
   end
end

% Size check
```

```
height= info(1).Height;
width= info(1).Width;

if height ~= width
   error('Image dimensions are incorrect')
end



 acporo=zeros(np,1);
for j= 1 : np
   if j==1
      A=zeros(height,width,lim);
      for i= 1 : lim
         A(:,:,i)=imread(tiffile,'Index',i,'Info',info);
      end
      B=(mean(A,3));
      B=B/255;
   else
      A_=imread(tiffile,'Index',lim+j,'Info',info);
      A_=im2double(A_);
      B=((lim+j-2)*B+A_)/(lim+j-1);
   end

   C=B;
%    To keep the B in memory untouched by the "cut" method for the next
%    iteration


% Image Scan/Matrix Cut Method
% Matrix scan from top to bottom
%  <0.95 works as a safety parameter: not all pixels in the outside are defined as 1
    for y = 1 : height
       for x = 1 : width
         if C(x,y)<0.95
            C(x,y)=NaN;
            break
         else
            C(x,y)=NaN;
         end
```

```
        end
    end
% Matrix scan from bottom to top
    for y = 1 : height
        for x = 1 : width
            a=700-x+1;
            b=700-y+1;
           if C(a,b)<0.95
               C(a,b)=NaN;
                break
           else
               C(a,b)=NaN;
           end
        end
    end

%

% Record of the mean and accumulated porosity
     acporo(j)= 1-mean2(C(~isnan(C)));

end
imshow(C)
% Plot of accumulated porosity vs number of pictures
%     plot(n,acporo,'+','MarkerSize',5)
%     n
%     acporo
%     ylim([0.35 0.38])
%     xlabel('N° of scans')
%     ylabel('Accumulated porosity')

End
```

```
function porovsr_matrixm(nfile,np,nim)
% Calculate and plot the mean porosity vs radius(distance from the center of the column)
% nfile - Numerical identidy for the TIFF file to analyse
% np   -  Number of points in the pretended plot
% nim  -  Number of images to be analised, must be lower or equal to the
%         maximum number of images in the TIFF stack, limited to the
%         cumputer's maximum RAM capacity

% Identify TIFF stack file from directory
list= dir('*.tif');
tiffile=list(nfile).name;

% Collect image size information
info=imfinfo(tiffile);
height= info(1).Height;
width= info(1).Width;

% Size check
if height ~= width
   error('Image dimensions are incorrect')
end

% Read all the selected images and average everything into B
   A=zeros(height,width,nim);
for i= 1 : nim
   A(:,:,i)=imread(tiffile,'Index',i,'Info',info);
end
   B(:,:)=(mean(A,3));
   B=B/255;

% Image Scan/Matrix Cut Method and record in double vector
% Matrix scan from top to bottom
%  <0.95 works as a safety parameter: not all pixels in the outside are defined as 1
    for y = 1 : height
       for x = 1 : width
         if B(x,y)<0.2
            B(x,y)=NaN;
```

```
            break
        else
            B(x,y)=NaN;
        end
    end
end

% Matrix scan from bottom to top
    for y = 1 : height
        for x = 1 : width
            a=700-x+1;
            b=700-y+1;
        if B(a,b)<0.2
            B(a,b)=NaN;
            break
        else
            B(a,b)=NaN;
        end
    end
end

   k1=0;
   k2=0;
   O1=zeros(width,2);
   O2=zeros(width,2);

% Matrix scan from top to bottom with Marking
     for y = 1 : height
        for x = 1 : width
          if isnan(B(x,y))
              if x==width
                  k1=k1+1;
              end
          else
              k1=k1+1;
              O1(k1,1)= x;
              O1(k1,2)= y;
              break
          end
        end
```

```
    end
% Matrix scan from bottom to top with Marking
    for y = 1 : height
       for x = 1 : width
          a=700-x+1;
          b=700-y+1;
         if isnan(B(a,b))
            if a==1
               k2=k2+1;
            end
         else
            k2=k2+1;
            O2(k2,1)= a;
            O2(k2,2)= b;
            break
         end
       end
    end

% Define cartisian coordenates, axis and true center of the column

%    O2=flipud(O2); % inverte o sentido do scan para esquerda->direita

% Eliminate the empty lines
   O2(~any(O2,2),:)=[];
   O1(~any(O1,2),:)=[];

   % Top and Bottom
   maxlin=min(O1(:,1)); %linhas / y
   minlin=max(O2(:,1));

   linmax=mean(O1(O1(:,1)==maxlin,2)); %coluna das linhas / x
   linmin=mean(O2(O2(:,1)==minlin,2));

   %Left and Right

%     O3=[O1;O2];

   maxcol=O1(end,2); %colunas / x
   mincol=O2(end,2);
```

```
colmax=(O1(end,1)+O2(1,1))/2; %linha das colunas / y
colmin=(O1(1,1)+O2(end,1))/2;

nmax=O2(1,1)-O1(end,1);
nmin=O2(end,1)-O1(1,1);

O3=zeros(nmax-1,2);
O4=zeros(nmin-1,2);
for i=1 : nmax-1
   O3(i,1)=O1(end,1)+i;
   O3(i,2)=O1(end,2);
end

for i=1 : nmin-1
   O4(i,1)=O1(1,1)+i;
   O4(i,2)=O1(1,2);
end
   O4=flipud(O4);

%Create axis and center
line1=[mincol colmin; maxcol colmax]; %horizontal
line2=[linmax maxlin; linmin minlin]; %vertical

slope = @(line) (line(2,2) - line(1,2))/(line(2,1) - line(1,1));
m1 = slope(line1);
m2 = slope(line2);

intercept = @(line,m) line(1,2) - m*line(1,1);
b1 = intercept(line1,m1);
b2 = intercept(line2,m2);
centercol = (b2-b1)/(m1-m2); % x
centerlin = m1*centercol + b1; % y

r1= sqrt((linmax-centercol)^2+(maxlin-centerlin)^2); % up
r2= sqrt((maxcol-centercol)^2+(colmax-centerlin)^2); % right
r3= sqrt((linmin-centercol)^2+(minlin-centerlin)^2); % down
r4= sqrt((mincol-centercol)^2+(colmin-centerlin)^2); % left

rp=min([r1 r2 r3 r4]);
```

```
imshow(B)
hold on
th = pi/180:pi/180:2*pi;
xunit = rp * cos(th) + centercol;
yunit = rp * sin(th) + centerlin;
h = plot(xunit, yunit);

hold off

ang= 2*pi()/720 : 2*pi()/720 : 2*pi();
r=rp/np: rp/np : rp;



O=vertcat(O1,O3,O2,O4);
O(:,1)=-(O(:,1)-centerlin);
O(:,2)=(O(:,2)-centercol);

rt=sqrt((O(:,1).^2) + (O(:,2).^2));
angt=zeros(length(rt),1);
angs=zeros(length(rt),1);
angc=zeros(length(rt),1);

for i=1 : length(rt)

  angc(i)=acos(O(i,2)/rt(i));
  angs(i)=asin(O(i,1)/rt(i));

  if  angs(i)>0
     angt(i)=angc(i);
  else
     angt(i)=2*pi()-angc(i);
  end

end

teta=rt/rp;

      tetaf=interp1(angt,teta,ang,'linear','extrap');
```

```
        i=0;
        j=0;

        for i=1 : np

                acum=0;
      nancount(i)=0;

                for j=1 : 720
        inc=interp2(1-centercol:1:700-centercol,1-centerlin:1:700-
centerlin,B,tetaf(j)*(r(i)*cos(ang(j))),tetaf(j)*(r(i)*sin(ang(j))));
        if isnan(inc)
           inc=0;
           nancount(i)=nancount(i)+1;
        end
                        acum=acum+inc;
                end
                poro(i)=1-(acum/(720-nancount(i)));
        end

   plot(r,poro);
   r
end
```